Biomedical Engineering Department

BACHELOR THESIS

DESIGN OF A MICROFLUIDIC CHAMBER TO GROW SKIN-ON-A-CHIP

Author: **Pablo Tostado Marcos**
Director: **Javier Rodríguez Rodríguez**
Co-Director: **José Luis Jorcano Noval**

Leganés, September 25th 2014

Project: Design of a microfluidic chamber to grow ‘skin-on-a-chip’
Author: Pablo Tostado Marcos
Director: Javier Rodríguez Rodríguez
Co-director: José Luis Jorcano Noval

TRIBUNAL

President: _____

Vocal: _____

Secretary: _____

Realizado el acto de defensa y lectura del Trabajo Fin de Grado el día 30 de septiembre de 2014, en la Escuela Politécnica Superior de la Universidad Carlos III de Madrid, acuerda otorgarle la CALIFICACIÓN de:

VOCAL

SECRETARIO PRESIDENTE

AKNOWLEDGEMENTS

At this point, I would like to thank every person that contributed in any extent, directly or indirectly, to the development of this project, that made me believe in the power of engineering more than ever.

In particular, I would like to thank the Biomedical and Aerospace Department, for all the technical support and facilities provided, able to transform my enthusiasm and thirst of knowledge into tangible results.

The laboratory team, for their infinite patience and availability, ready to share their knowledge, to answer any little doubt at any time, and to forgive mess after mess. Thanks to Marta García Díez.

Of course, I would like to thank my tutors along these hard months in a very distinctive manner, Javier Rodríguez Rodríguez and José Luis Jorcano Noval. For your never-ending persistence to pull knowledge out of my brain, for your tolerance explaining everything twice, for making this happen.

Finally, I would like to dedicate this project to my friends and family, especially my parents and siblings, for all the unreserved support they gave me throughout my university career, trusting me and encouraging me to do something meaningful. Nothing would have been possible without your endless help.

To all of you, thank you.

This project was developed at the Polytechnic University Carlos III of Madrid, under the supervision and guidance of Javier Rodríguez Rodríguez and José Luis Jorcano Noval.

INDEX

Outline of the document

The present document is organized in 6 chapters. Chapter 1 and 2 present the biological motivation of the project and its main objectives. In chapter two, an introduction to the background of the problem necessary to understand the key concepts of the project is exposed. Chapter 3 carefully describes the protocols followed, the software used and the broad statement and solution of the problem. In chapter 4, the results are presented and objectively discussed. Chapter 5 contains the conclusions and future perspectives of the approach.

1. MOTIVATION AND OBJECTIVES

1. Motivation and Objectives

1.1. Biological motivation

Since the birth of molecular biology, science has always tried hard to figure out the ways to enter the human body and gain insightful information about its metabolic activity and cell behavior.

However, human biology is complex. The human body functions over a multifaceted interaction amongst a long list of working organs that perform different biological tasks.

The difficulty digging into the cellular tissues of living organisms together with the limited laboratory techniques to reunite and reproduce the physiological conditions present in the body make the advance in human physiology knowledge a slow process.

In addition, there are constraints in the evidences that can be inferred from single-typed cell cultures. Isolating a certain cell-type from a target organ and studying its behavior in the laboratory may provide significant information. Nonetheless, as soon as it is isolated, the interaction of the aforementioned cell-type with the rest of the cells present in the surrounding body is suppressed. Therefore, it is not possible to acquire all the necessary information about the cell behavior under different physiological conditions.

These restrictions in the reproducibility of an accurate physiological environment have driven scientists all over the world towards a desire to transmit the communication between cells, tissues and organs to the lab in order to gain a better understanding of all the biological processes taking place within the human body.

This aim to develop and reproduce all the physical and physiological factors that govern the behavior of a specific organ in vivo led to the concept of '*organ-on-a-chip'* (OC). An OC refers to a multichannel 3D microfluidic cell-culture chip capable of mimicking the activity, mechanics and physiological response of a whole organ system in vitro. (1, 2)

The idea of developing different types of organs-on-chips collapses into a bigger picture: a '*human-on-a-chip'*. The final goal would be to integrate all this organs-on-chips together in order to be able to accomplish a global interaction among engineered organs reproducing the metabolic behavior of the entire

human body, to create a homunculus(3). Homunculus is a miniature representation of a real human.

But, what is the motivation of such a project?

Being able to reproduce the human body in the laboratory would have an endless number of scientific applications, the most outstanding being there:

- Understand human physiology.
- Advance in the comprehension of environmental toxicology.
- Improve drug development.

It is the simplification-of-drug-development application where organs-on-chips have the most significant impact. The way new drugs are currently discovered and developed is too costly, too slow, and inefficient. This constitutes a global health challenge that delays the development of new therapies for disease treatment. The following figure shows the decline of R&D productivity over the past years.

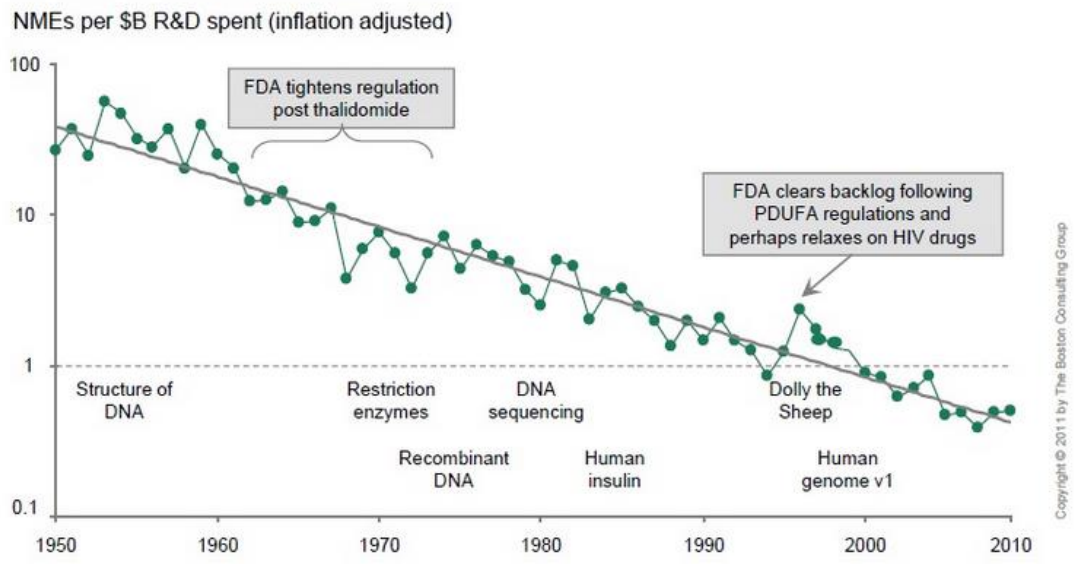

Figure 1. Number of new drugs per $B of R&D spending. (4)

One of the key factors affecting the inefficacy of drug development is that the tools that are available to test whether a new drug is safe and efficient are unable to predict the workability and applicability of the new medicaments.

The process that must be followed to test a new drug before it can be launched into the market involves:

- ✓ **Petri dishes:** The drug is tested on a target cell-culture into the lab.
- ✓ **Animal testing:** Usually mice are used to assess the response of the organism.
- ✓ **Human trials.**

Yet, the first two steps often fail to predict the human response to a new drug, leading to adverse drug reactions. As explained before, cells in petri dishes have been ripped out of their native environment and not receive any physiological stimuli; hence their response does not correspond to the one in the body. In a similar way, even though animal models provide useful information about the response of a complex integrated living organism, their genetic information is different from that of the humans and therefore animal tests are frequently inaccurate and distrustful.

Consequently, the development of organs-on-chips supposes a great advance in the process of drug testing, reducing the controversial dependency on animals, and yielding more realistic, predictive results about the human response. It is important to understand that an OC is not aimed to have the same physical features of the organ it mimics, but it is an engineered device in the microscopic scale that recreates the smallest functional unit that represents the biochemistry, mechanics and function of the cells of the organ in the body.

Studies have already been performed with an engineered '*lung-on-a-chip'* in the University of Harvard; where actual white blood cells from the immune system reacted towards an intentional bacterial infection. (5)
The final goal would be to achieve sufficient functionality by the interconnection of these different OCs in order to obtain trustful information about what would happen when a drug enters the body being absorbed (through the skin), being inhaled (through the lungs), eaten (through the stomach) or intravenously (through the blood) and how any other organ would react to it.

1.2 Objectives

The goal of this project is the design of a microfluidic chamber to grow skin-on-a-chip. To do so, several software tools will be used to develop, analyze and compare different approaches to the problem in order to define the model characteristics that best fulfil the required functionalities.

2. INTRODUCTION

2. Introduction

Since molecular biology was born, there has been a growing motivation to be able to simulate and reproduce the biological conditions that are found in living organisms in order to develop stable cell cultures in vitro.

The capability to sustain viable cultures by replicating live-like conditions supposed a huge step in the path to comprehend how cells behave, communicate, interact or respond to external stimulus.

From that point on, there has been nothing but an exponential flood of biological information that we have collected, analyzed and mastered in order to guide cell replication and cell growth towards target goals. We are now able to expand epithelial tissues for skin transplants, to target cell differentiation from pluripotent stem cells (PSCs), or to promote cell-cell interactions as desired. (6)

However, there is still a long road to explore until we reach the degree of complexity that may be found into pluricellular organisms as it is the case of the human kind.

Different fields such as molecular biology and engineering work now together with a common objective: to study, understand and build living-like structures and engineering masterpieces that take advantage from the biological principles that occur in live and reproduce them artificially in vitro.

2.1. The integumentary system

The human body is a nearly-perfect engineered machine composed of different organs that form systems which fit together allowing life to occur. Every system in this harmonic union has a determinant function without which life would not be possible. When we are asked about the most important organ in the body, we immediately think about those organs whose purpose is most astonishing. However, those organs could not develop their role deprived of the functions of the surrounding systems. In this project, we will be dealing with one of the most significant structures regarding the protective function: the skin.

The integumentary system is described as the organ system in the body that serves as a separation barrier involving the inside and the outside of the body. It is in charge of several functions, including impermeability, waterproof, insulation, temperature regulation, excretory function and specially protection against different damages from the outside world, such as loss of water or abrasion. It is important to mention that it also holds the sensory receptors necessary to get information from the outside and transmit it inwards.

The integumentary system, in the case of the human species, is formed by the skin and its appendages: hair, nails and associated glands.

Its main component, the skin, is known to be the largest organ found in the body. From the inner to the outer layers, we may define the structure of the skin as follows:

- **Fat layer:** On the basis of the skin, below the dermis, a layer of fat is located that helps insulate the body and maintain a constant inside temperature, provides protective padding, and serves as an energy storage area. It is formed by the so-called adipocytes, which contain the fat in their inside and are held together by fibrous tissue.

- **Dermis:** The skin's next layer is the dermis. It consists of a thick layer formed by fibrous, elastic tissue made of elastin, collagen and fibrillin. Its main function is to confer flexibility and strength. It also contains some other important components such as sweat and sebaceous glands, hair follicles, blood vessels or nerve endings.

- **Epidermis:** The outermost skin's layer is called epidermis. This thin, tough part of the skin is mainly composed by keratinocytes. Originated in the basal layer (*see Figure 1*), keratinocytes emigrate toward the surface of the epidermis as they differentiate. Once they reach the surface of the skin, they are gradually replaced by newer cells. By this mechanism, the cells forming the skin are being constantly renewed. The outermost slice of the epidermis, the stratum corneum, consists of dead cells, (corneocytes), and is in a great part responsible for the vital barrier function of the skin. Even though it was thought to be biologically inert, recent studies have shown that the stratum corneum has an intricate and complex biological and chemical activity that contribute to the protection of underlying tissue from dehydration, chemicals, infection, mechanical stress and others.

Located within the basal layer, we also find the melanocytes, which produce melanin (pigment responsible of the skin color), which filters out the ultraviolet radiation preventing DNA damage to the underlying cells.

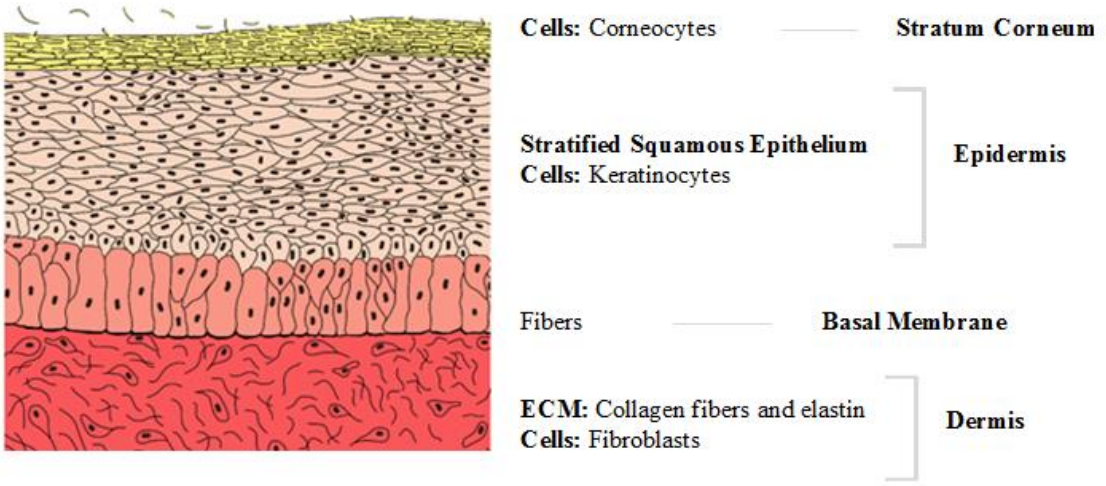

Figure 1. Structure of the skin's stratified layers and their composing main cells.

2.2. Introduction to Tissue Culture

Scientists have always attempted to cultivate cells separate from the organism. Tissue culturing refers to the process by which isolated cells from a multicellular organism are grown in vitro. Nowadays, there is an endless number of cells that can be isolated and cultured in the laboratory. However, due to the easy access to the skin, culturing dermal cells might be one of the most mastered and common processes regarding cell cultures.

Culturing techniques have been developed since the first cell culture was performed in the beginning of the 20th century. It was the demonstration that each cell type responds best to a different optimal mixture of nutrients that supports its function what led to the development of culturing media characteristic for each cell. Moreover, the addition of defined components such as proteins, hormones or growth factors opened a new wide range of possibilities to control and address the culturing techniques. (7)

Presently, the cells are usually bathed in a culture medium that contains all the essential nutrients and growth factors necessary for the cell's survival and differentiation. *Figure 2* shows some typical instruments used to grow tissue in vitro.

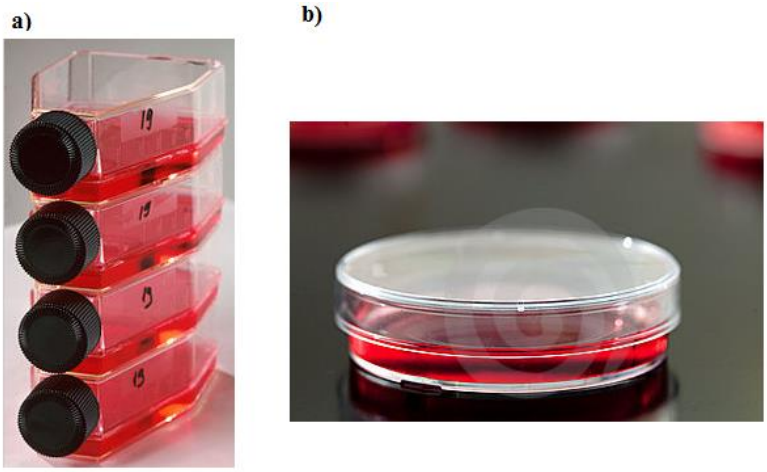

Figure 2. Laboratory flask **(a)** and petri dish **(b)** containing growing medium for cell nourishment in tissue cultures.

Cell-culture procedures aim to grow living cells under controlled conditions, generally outside of their natural environment, with the objective of understanding and testing the processes involved in cell replication as well as cell-cell interactions.

In modern molecular biology, cell culture systems are widely used as a tool for basic research and clinical in vitro studies. In the beginning, cell cultures were based on a 2D growing method, usually making use of a petri dish. This method allows scientists to comprehend different single cell type's behavior that would be unknown otherwise. However, even though static 2D culture systems are used as reference models, they often result in unsatisfactory, non-predictive and misleading data for in vivo response due to the fact that they poorly mimic the conditions that are found in living organisms. These limitations restrict the significance of the results obtained from such approaches.

Hence, molecular biology has evolved towards more reliable methods for cell-culturing processes by developing 3D models that embrace living-like conditions in which biological cells are permitted to interact with their surroundings in all three dimensions.

2.3. From 2D to 3D cultures

Until recently, most of the studies concerning cell-cell interactions have relied on 2D cell-culture models, due to the difficulty to build more complex, viable environments. The problem is that these models fail to reconstitute the biological environmental conditions that are found in vivo, which leads to an

impossibility to maintain the differentiated functions and natural cell growth of in vitro cultures.

As stated before, in order to fully understand the functioning and formation of tissues, it is critical to study them as part of whole living organs, in which different tissue types interact dynamically.

Aware of the limitations originating from the basic 2D cell cultures, great efforts have been made in order to develop 3D models able to comprise the necessary characteristics of natural tissue formations. In the case of 3D cultures, cells are grown within microfabricated ECM gels that mimic tissue and organ-specific microarchitecture. Not only this technique improves tissue organization, but the differentiated functions of the cultured cells are also preserved. (8) (9)

Nevertheless, even if this new type of structure overcomes some of the limitations posed by 2D techniques, 3D models still fail to reconstitute most of the features characteristic of living organs that are crucial for their purpose. These include tissue-tissue interfaces that cooperate for the organ function, mechanically active microenvironments or spatiotemporal gradients of chemicals and oxygen.

2.4 From 3D cultures to organs-on-chips

The next step in the race to overarch all the necessary features of real organs in vitro in order to approach human physiology is the so-called organs-on-chips. This new development based on microengineering techniques is the next generation of 3D cell-culture models, which better mimic the structural microarchitecture, the dynamic physiological properties and biological functionalities of whole functional organs. The goal to achieve is to reconstitute all the physiological characteristics of living organs by reproducing tissue-tissue interactions, biochemical gradients present in vivo and replicated microstructure, in order to obtain a living-like behavior for system-level analysis. (10)

With these approaches, the possibilities for cell disease analysis, developments of disease models or drug testing experiments are immediately enhanced, reducing the current unavoidable reliance on time-consuming, costly animal study, which often fails to produce useful data for human application.

The design and fabrication of these devices in the microscale require the integration of two main fields: **microfluidics** and **microfabrication.**

One of the core fields of study involved in the development of these organs-on-chips is microfluidics. The capacity to manipulate and control small amounts of fluids in hollow channels is used to generate and precisely tune both dynamic fluid flows and spatiotemporal gradients in microengineered devices as well as to deliver nutrients to cells seeded in the chips. (11)

In addition, owing to their small size, fluid flow in microfluidic devices is entirely laminar. This means that the fluid flows in parallel layers with virtually no mixing between neighboring streams. This property allows for the generation of abrupt step gradients to deliver gradients of chemicals across the diameter of a single cell, or to study cell motility in response to chemotactic stimuli.

These microfluidic devices can be constructed in order to develop controlled microenvironments. Some of the most astonishing examples of the complex microengineered instruments that have been developed include, for example, a microdevice containing a cross-flow bioreactor able to maintain efficient oxygen delivery and physiological levels of shear stress for 3D reorganization to study the metabolic demands of rat hepatocytes, a PDMS microfluidic system for toxicology studies on liver epithelial cells or a self-contained microcirculating cell-culture system to analyze human vascular endothelial cell responses to hemodynamic stresses .

In addition, microfabrication techniques can be combined with microfluidic designs in order to generate patters and structures that provide more physiologically relevant cell-culture conditions.

The final step for the design of the so-called organ-on-a-chip is the integration of biological functionality to these microdevices. Organ-on-chip microsystems reproduce key structural, functional and biomechanical features of real living organs into a single device. The most recent designs in the field include a mammary gland-on-a-chip, a kidney-on-a-chip (12), a brain-on-a-chip(13), a gut-on-a-chip (14), or lung-on-a-chip, (15) the latter being analyzed in the following section.

As stated before, the final step will be to integrate all these compartments in order to obtain a ‘human-on-a-chip’ linked through a microfluidic circulatory system that reproduces ideally full functionality of the human body.

2.5 Lung-on-a-chip

Undoubtedly, one of the smartest and successful examples of these microfabricated devices consists of a lung-on-a-chip developed by a research group of the Harvard University. (16)

This biomimetic microsystem reproduces key structural, functional and mechanical properties of the human alveolar-capillary interface of the lung. The design of the lung-on-a-chip is defined by the integration of two lateral microchambers and a microfluidic system containing two parallel microchannels separated by a thin porous membrane. The membrane was coated with fibronectin ECM to sustain a human alveolar epithelial cell- and a human pulmonary microvascular endothelial cell-culture at opposite sides. The structure of the design is represented in *Figure 3.*

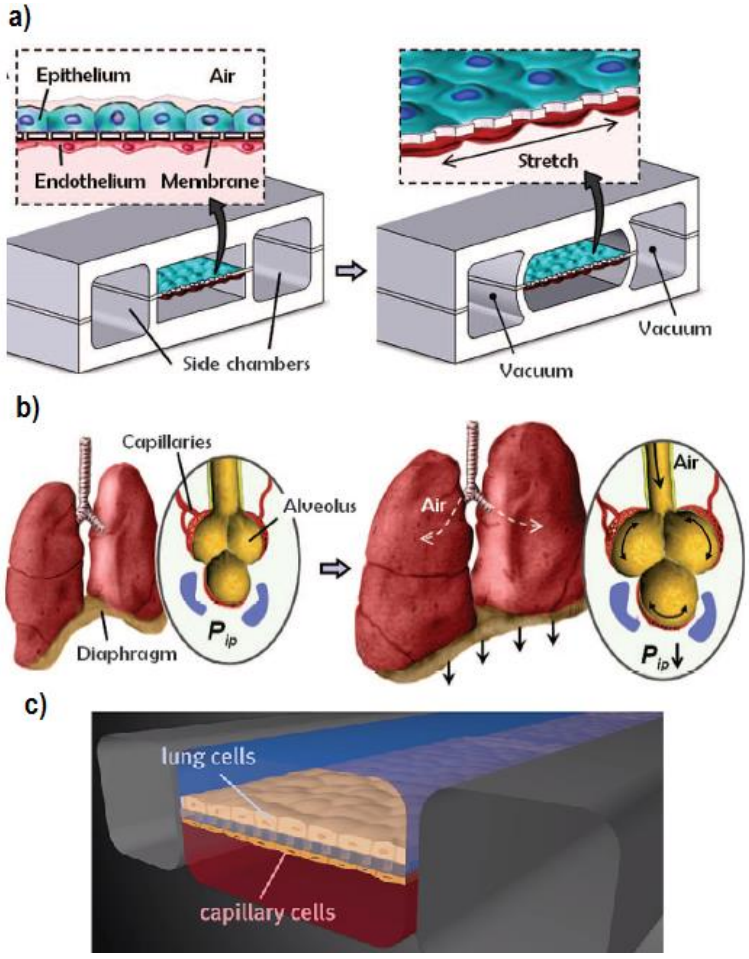

Figure 3. 'Biologically inspired design of a human breathing lung-on-a-chip microdevice'. (The microfabricated biochip uses a porous PDMS membrane coated with ECM to form an alveolar-capillary barrier that imitates the lung epithelium-endothelium interface **(a).** During inhalation, (simulated by vacuum application through the hollow aside microchannels) the PDMS membrane is tensed mimicking the expansion of the alveolar-capillary interface in a real lung **(b).** A computer simulation from the Wyss Institute is shown in figure **(c).** (12)

The aforementioned microchambers were included in order to mimic the pressure-driven stretching of the alveolar epithelium and endothelium when air goes into the lungs during inspiration. It is accomplished by causing the elastic deformation of the PDMS permeable membrane, (and consequently of the adherent tissue layers), when vacuum is applied to these chambers. The design replicates the dynamic mechanical distortion of the alveolar-capillary interface during respiration.

This model revealed significant results related to toxic and inflammatory responses of the lung to silica nanoparticles, as well as mechanical information to enhance and stimulate the uptake of nanoparticulates.

2.6 Skin-on-a-chip

The goal of the present project is to design a microfluidic chamber that imitates the functional, structural and biomechanical physiology of the skin. The model will contain a two-layered structure aiming to simulate the dermis and epidermis interface, as well as a set of engraved microchannels in an attempt to provide nutrient supply.

Different inspirations lead to the implementation of this task. There is a myriad of possible applications of the skin-on-a-chip.; for example:

- It could be intended to cover prosthetics. The unaesthetic and unnatural appearance of prosthetic devices could be solved by coating them with a vascularized, living artificial skin that can even be developed from own cells of the patient.

- It could serve as a coating for robotic arms. One of the most important drawbacks of robotic arms in the lab originates from the difficulty to confer accurate sensibility to the environment. Robots could be equipped with an extracorporeal vascularized skin to enhance temperature, roughness or patterning sensibility.

- Finally, as it has been claimed, the main application of the design would be related to drug screening in the implementation of the so-called project: '*Human on a chip'.* The development of organ-on-chips devices to better predict the human response to new medicaments would not only improve the reliability of the testing results, but it would also replace animals for drug testing and accelerate and cheapen the new pharmaceuticals development processes.

3. MATERIALS AND METHODS

3. Materials and Methods

3.1. Software and programs

MATLAB was used as mathematical software to perform all the calculations and simulations of the developed models, as well as to display the graphical results.

PDE interactive tool in Matlab was used as the basis to draw the 2D mathematical models, set, and solve the partial differential equations.

SketchUp software to implement 3D simulations of the different models.

3.2. Statement of the problem

The goal of this project is the design of a microfluidic chamber that mimics the mechanics of the skin in vivo.

In the past few years, there have been many examples of different attempts to create bioengineered models to reproduce this organ in vitro. (17)

In this project, it is developed a model that has a well-defined microengineered structure consisting of a permeable gel within which microtubes are engraved simulating the blood vessels. Through the aforementioned microtubes, there is a constant flow of nutrients that diffuses all through the gel. This model simulates the structure of the dermis in the skin. The composition of the different parts of the device is described in the following section.

3.2.1 Device structure

In this first approach, we describe the simplest structure possible for a microfluidic device to grow skin cells following our model. The components of such a structure are enumerated and shown below (*Figure 4*).

- **Microfluidic channels.** On the lowest part of the device, the symmetric microfluidic channels through which the flow will take place are located. There will be two different senses of circulation that happen in alternate channels, one containing the nutrients' support necessary for cell growth, and the other containing pure serum that collects the waste products resultant from the cells' metabolism. The flow will take place from the formers to the latter as desired, due to a designed pressure difference.

- **Permeable fibrin gel.** The flow will occur though a porous fibrin gel of engineered permeability and dimensions. The cells will be seeded within the aforementioned gel, and will be the target of the created flow.

- **Impermeable membrane.** In early stages, it might be necessary to include an impermeable membrane on the top of the device to avoid the loss of flux through the top, which is exposed to the atmospheric pressure, before keratinocytes may be cultured.

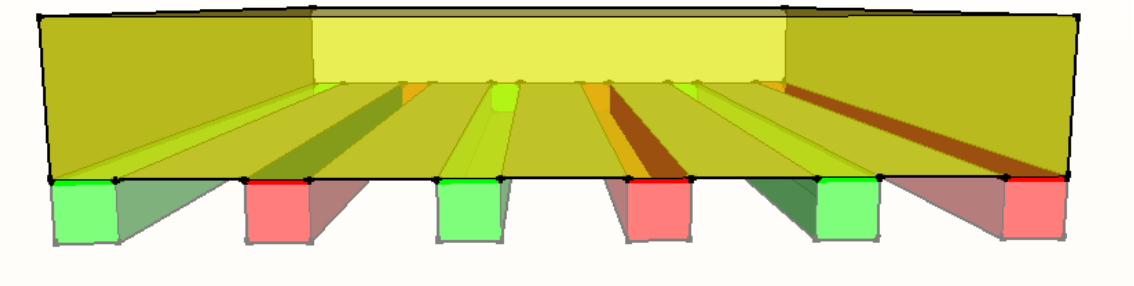

Figure 4. Simulation of the design of a microfluidic chamber for skin growth. Components: Permeable fibrin gel (in yellow), and alternated channels of nutrients supply (in green) and trash removal (in red).

3.2.2 Flow parameters

The first step in the design of the microdevice is to analyze and stablish adequate, realistic values for the parameters defining our model. Some of the parameters may be variable and engineered as desired, and some others will be intrinsic of the model and materials used.

In this first stage, we will assume that the device consists of a structure containing two layers: a bottom layer of solid impermeable material where the channels are located, on top of which the diffusive gel will be located. The layers must be as transparent as possible, and cover an area L x L. The separation between channels is prescribed, and defined by the parameter W. This W must be adequate to suffice the minimum flow intake required by the cells. The number of channels will be N = L / W. Supply and trash removal channels will be intercalated, so each channel of one type is enveloped by two channels of the other type.

Both layers are briefly described as follows:

1. Rigid base where the channels are engraved. The dimensions of this layer are not important, as long as it is large enough to hold the depth of the channels D. Its permeability is null, so that the only allowed escape to the flow is through the gel.

2. Fibrin gel of base L x L and thickness H, with ideally constant permeability K. This permeability will be chosen and varied by the desired crosslinkage. It will mimic the dermis and hence will be populated by fibroblasts.

Regarding the engraved channels, they will be designed to have a square cross-section of side D, with the only constraint being D << W. As mentioned before, channels of different types will be intercalated. The direction flow may be chosen to be either on the same sense or opposite to each other, as long as the pressure difference at every cross-section promotes a flow of fluid from the positive (nutrient-containing) to the negative (waste-removal) channels.

The whole list of parameters is listed below:

- **Positive Pressure (Pp).** This is the pressure gradient applied to the '*positive channel'*, through which the nutrient flow goes. The important fact is the initial value given to Pp on the entry of the positive channels.

- **Negative Pressure (Pm).** This is the same parameter as Pp but applied to the waste-collecting, '*negative channels'*. The values given to both parameters are not as important as the difference between them, Pp-Pm, which will be the motor of the fluid flow through the fibrin gel between both channels.

- **Dynamic Viscosity (μ).** This parameter defines the viscosity of the flow through the channels.

- **Density (ρ).** It refers to the fluid's density.

- **Gel length (L).** This parameter defines the total length of the gel, and therefore, that of the engraved channels. This length should be chosen consciously according to the desired culture area that we want to obtain, but it should not affect the results of the calculations. If both base dimensions of the device are set to L, it will cover an area of L x L.

- **Side of the channel (D).** The side of the channel that will define its cross-section D^2 will be chosen according to the desired amount of fluid we want them to hold, respecting the microfabrication techniques available for its construction.

- **Channel Separation (W).** The channel separation is defined as the distance between the middle points of two adjacent channels. It must be selected so that the diffusive flow through the fibrin gel is enough to nourish every cell.

- **Number of channels (Nc).** In this first approach in which we only have one layer of channels, the number of channels will correspond to the length of the device L divided by the distance between channels. (Nc = L/W).

- **Thickness of the fibrin gel (H).** The height of the gel is important, especially in this primitive model in which we only have one layer of channels. That means that the area covered by the flow escaping from the channels is limited in height, and this must be taken into account. In the following models, this will not be a problem, since the nutrient supply's reach will not be limited.

- **Permeability of the fibrin gel (K).** This is perhaps one of the most important parameters of the model. It will greatly influence the spread of the flow through the porous gel, and will have a major effect in the diffusion of the nutrients that must reach the populating cells. Its value will not be as variable as desired, since the consistency of the gel depends on it, and it can only be modified by varying the crosslinkage included in the formation of the fibrin gel.

- **Friction coefficient of the channel (f).** This parameter is related to the loss rate, and its value depends on both the geometry of the channel and the Reynolds number of the flowing fluid. It must be calculated experimentally for each different geometry.

3.2.3 Physiological parameters

For the in-vitro skin model to succeed, it must work as close to the skin behavior as possible. In this section, we discuss some of the factors to be taken into account in the design and simulations of the model. However, the selection of the appropriate parameters' values will be done by computational simulations.

Some of the parameters that will be pretty stable depend on the materials used. The first values that must be known are the dynamic viscosity and the density of the fluid. In the project, we assumed a probable similarity to those of the water at 30ºC, μ = 0.79 E-3 [N.s / m^2], ρ = 995.7 [Kg / m^3]. Also, we need to know the loss coefficient of the channels, which is related to their geometry. Experimentally calculated values for non-circular pipes can be found in tables. For instance, the friction factor for squared-sectional pipes is f = 56.91/Re [Dimensionless].

Some other parameters will be variable, and can be chosen arbitrarily, such as the dimensions of the device. However, they must ensure that the nutrient supply is enough for every cell within the fibrin gel. To do so, we based an initial estimation of these parameters based on physiological data from the body. Researchers estimate that no cell is further than 0.01 cm (100 μm) to a capillary. According to this assumption, standard values of H, W and D in the range of μm were chosen. In order to calculate the Reynolds number described afterwards, we need the average velocity of the fluid. In a first approach, the average velocity of the fluid in a capillary was chosen, v = 0.65 mm/s. According to this data, and taking into account the cross-sectional area of the channels (v = Q / A), an initial flow input of Qo must be calculated in order to satisfy the requirements of the model.

Also, the pressure difference between the channels can be inferred from the physiological pressure difference existing between the capillaries and the surrounding tissue which, according to widely accepted literature, is ΔP = 10 Torr, ~1300 Pa. (18) A pressure-difference value in this range will be selected.

Finally, we had to consider the permeability of the model. In a first thought, the permeability of the extracellular matrix of the dermis could be an appropriate value. However, the fact is that the capillary walls serve as a barrier to the blood compounds preventing them from diffusing all around. In our model, the channels are totally open to the gel causing a diffusion enhancement. This effect could be counteracted by either reducing the nutrient-concentration of the flow, or by reducing the permeability of the fibrin gel compared to the biological values. In any case, the permeability of three-dimensional fibrin constructs correspond to fibrinogen and thrombin concentrations. Literature shows common values of the permeability coefficient of K = 2e-12 cm^2. (19)

3.2.4 Flow description

The goals of the calculations performed will be to satisfy the conditions of the design, that is, to ensure a flow field in the fibrin gel that guarantees that the cells embedded in the gel (fibroblasts) and those lying on top of it (keratinocytes) are supplied with enough nutrients, maintaining a sufficient trash removal rate to allow normal cell development. At the same time, we need to be sure that the pressure gradients imposed in the channels allow for flow movement while keeping the integrity of the device untouched.

With these ideas in mind, we will make the following assumptions that will allow us to look at the problem from a simplified point of view and perform the necessary calculations:

- **The flow will be assumed to be fully dominated by viscosity.**

In fluid mechanics, the behavior of a fluid may be classified into two main groups: laminar flow or turbulent flow. In general, we say a flow is laminar or streamline when a fluid flows in parallel lines (avoiding mixing) with no disruptions among them, whereas it is said to be turbulent when it has chaotic property changes regarding pressure or velocity in space and time. Of course, there is not a certain point at which a flow stops being completely laminar in favor of a turbulent behavior. In contrast, there exists a progressive transition by which a fluid starts losing the characteristics of a laminar flow and starts behaving turbulently. (20)

The manifestation of such characteristic types of flow is related to the predominance of either inertial or viscous forces. This relationship is described by the so-called *'Reynolds Number'*, a dimensionless quantity that is often used to predict similar flow patterns in different flow situations. The general formula for this number is:

$$\mathrm{Re} = \frac{Inertial\ Forces}{Viscous\ Forces} = \frac{\rho v L}{\mu} = \frac{vL}{\upsilon}$$

- $\boldsymbol{v}$ is the mean velocity of the object relative to the fluid [m/s]
- **L** is a characteristic linear dimension, (travelled length of the fluid) [m]
- $\boldsymbol{\mu}$ is the dynamic viscosity of the fluid [$N{\cdot}s/m^2$]
- $\boldsymbol{\upsilon}$ is the kinematic viscosity ($\upsilon=\mu/\rho$)[m^2/s]
- $\boldsymbol{\rho}$ is the density of the fluid [kg/m^3]

Even though there are different unmatched criteria on the limits to consider what a laminar and a turbulent flow is, most of sources consider laminar flows for Reynold numbers below 2300, and turbulent flows for Re > 4000.

In any case, if we consider our flow to be fully governed by viscous forces, which means the Reynold's number will be small, we may assume that the flow will be laminar.

- **The flow will be assumed to be slender.**

Slenderness is the feature of bodies or systems having little width in proportion to length or height.

In fluid dynamics, the slender-body theory is a methodology used in slender systems that takes advantage of this property in order to obtain approximations to a field surrounding it. This means that we will neglect the derivatives of the flow field when we calculate the effect of such a field in different cross-sections of the channels. We will only take the longitudinal dimension into account when calculating the pressure gradient and the rate of variation of the flow rate transported along the channels. As we have explained, for this approximation to be valid, the transversal transport of fluid must be small compared to the longitudinal one, and this condition is satisfied at very low Reynold numbers (Re~0) , (21) as we verified in this work.

- **Problem description**

Once the conditions have been stablished, we proceed to pose the problem.

In mathematics, the Laplace's equation is a second order partial differential equation (PDE) derived from the elliptic PDEs type. Elliptic PDEs have the following form:

$$- \nabla (\varepsilon * \nabla \cdot (\varphi)) = \rho$$

Due to the assumed hypotheses, the distribution of pressures will satisfy the Laplace's equation in the transversal plane (y-z). This is due to the two laws that describe our model. First, it is a porous medium with low Reynolds number so it satisfies Darcy's law: $\vec{v}$ = (-k/μ) ∇P. Secondly, it is incompressible, so $\nabla \cdot v = 0$. Consequently, we end up with the following PDE to be solved:

$$\nabla^2 \varphi = 0$$

The next step is to define the geometry on which the partial equation applies. We need to define the simplest region of the device that serves as the basis for the whole construction. This region is the smallest symmetrical region that repeats along the structure, and goes from the middle of one positive channel to the middle of the immediately adjacent negative one. The solution to the problem in this region will govern the performance of the whole model.

Finally, in order to be able to solve the PDE, the boundary conditions must be specified. In general, two types of boundary conditions may appear: Dirichlet and Neumann boundary conditions. Dirichlet (or first-type) BC determine the values that the solution of the PDE must take along a boundary of the domain. In contrast, Neumann (or second-type) BC specify the values that the derivative of the solution to a PDE must have along the boundary it applies to. In our problem, we imposed first-type BC in the channels' regions in contact with the gel (Pp and Pm) and at upper boundary (top of the fibrin gel in contact with the atmosphere), stating that the pressure at this boundary must be P = Pa. However, we took this value as a reference to the whole problem, and set it to P = 0. The rest of the points have pressure values related to this standardized scale. In contrast, Neumann boundary conditions apply to the rest of the borders of our domain, indicating that no flux occurs through the limiting walls. *Figure 5* shows the problem we described.

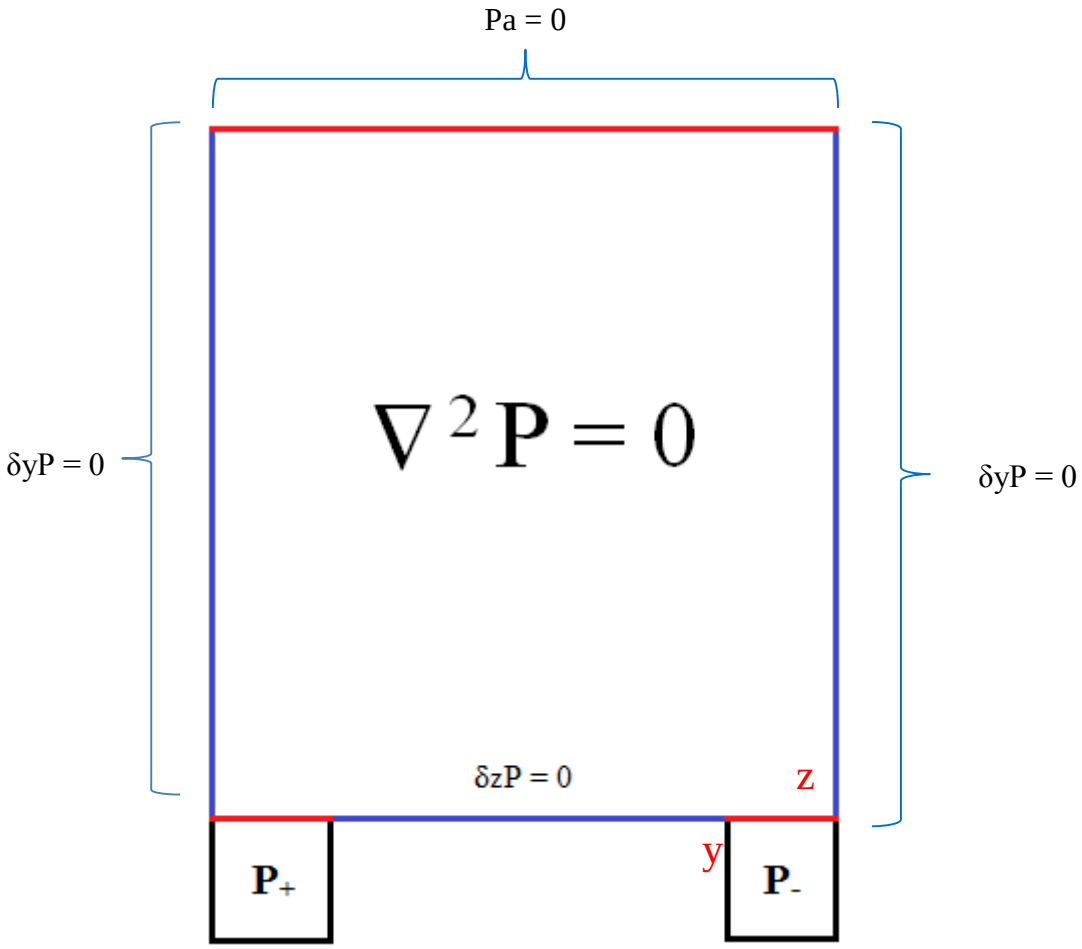

Figure 5. Cross-sectional region of the problem to which the Laplace's equation applies. The Dirichlet (in red) and Neumann (in blue) boundary conditions are depicted in the figure.

The problem was solved in two ways, analytically and programmatically.
In the following section, the analysis of the solution method using specific software is described.

3.3. Solution to the problem

The problem that must be solved was stated previously *(Figure 5)* for our target geometry. As we have explained, the Laplace's equation applies. Even though the problem was solved analytically for the pressures using separation of variables in a first attempt, the project was finally developed using a Matlab tool that is intended to solve PDEs in described geometries.

However, some of the analytical solutions will be used to evaluate important parameters of the flow, for instance, the main equations that govern how the pressures and the flow rates change along the channels. Once the pressure field is computed, we will be able to evaluate these variations along the longitudinal direction of the channels.

(1) $$\frac{dP+}{dx} = -\frac{\mu f}{D^4} Q_+$$

(2) $$\frac{dP-}{dx} = \frac{\mu f}{D^4} Q_-$$

(3) $$\frac{dQ+}{dx} = -\frac{D\bar{K}}{\mu W} \Delta P$$

(4) $$\frac{dQ-}{dx} = \frac{D\bar{K}}{\mu W} \Delta P$$

Figure 6. Variations of the positive (1) and negative (2) pressures along the longitudinal direction, and of the flow rate in the positive (3) and negative (4) channels due to the pressure difference (Pp-Pm).

These set of four differential equations will be the basis to evaluate important changes in the pressure and flow rate along the channels. However, the $\vec{K}$ operator is an equation factor that relates the flow rate loss (dQdx) with the difference in pressure applied. Therefore, it depends on a wide range of factors involving the geometry of the model, the permeability of the gel, the initial conditions etc. It obviously varies along the pipes, and would have to be calculated experimentally. Due to the impracticality of the process, the problem will be assessed in a different manner. The flow rate losses (dQ_+dx and dQ_-dx) will be repeatedly calculated numerically for different (x). In a parallel way, equations (1) and (2) will be used to study pressure changes for differential steps dx.

3.3.1 PDE tool

The Partial Differential Equation Toolbox (PDE Tool) developed by MathWorks provides a set of tools for the study and solution of PDEs in a 2D specified geometry and time.

In our case, it is highly useful so as to the study of the distribution of pressures in a defined cross-section of (y-z) at any point of the longitudinal dimension of the channels (x). The application display is shown in *Figure 7*, and it illustrates the different options that may be found when posing a problem with PDEs involved.

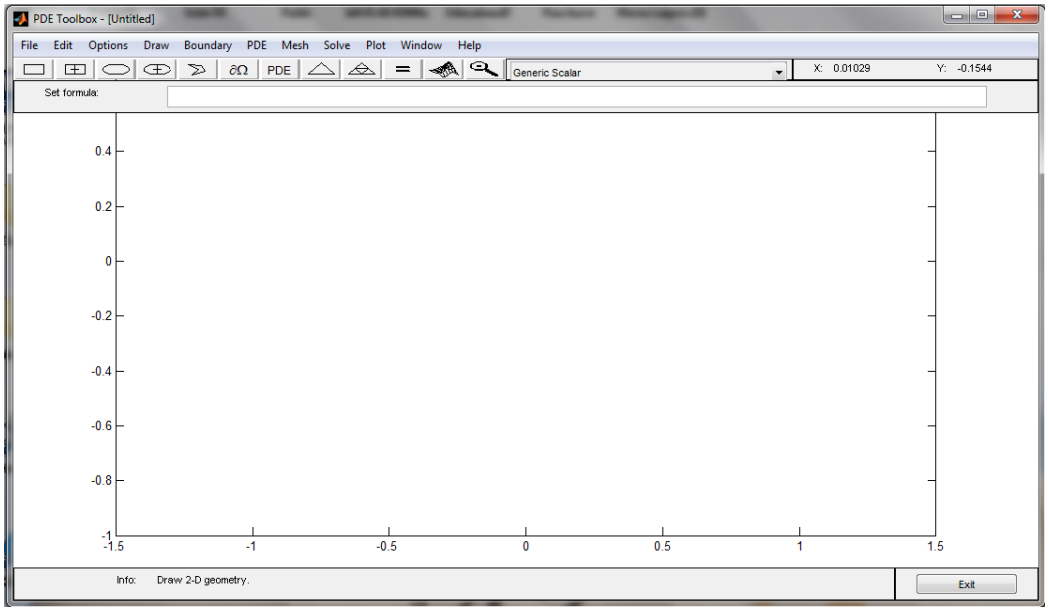

Figure 7. PDE-tool display to draw and solve PDEs in 2D domains.

In the description of any problem, we need to follow the steps explained below:

- **Description of the problem geometry.**

The first step consists of defining the 2D geometry to which the PDE applies. The application has several possibilities to do so. In our model, the desired geometry consists of a polygon involving the basic symmetry that repeats over the y-z space, which takes one channel of each type from their middle points and the height of the fibrin gel. The geometry is depicted in *Figure 8a.*

- **Specify the PDE to be solved.**

The next step would be to specify the type of PDE that applies to our model. As discussed before, the pressure field of our problem responds to the Laplace equation, which is a special case of the electrostatic equation. We have chosen the electrostatic equation: $- \nabla (\varepsilon * \nabla \cdot (\varphi)) = \rho$, with coefficients $\varepsilon = 1$ and $\rho = 0$;

- **Specify the boundary conditions of the problem.**

As a requirement of any problem involving PDEs, the boundary conditions must be specified to get the specific solution for each problem. Using the '*Boundary Mode'* of the PDE tool, we depict the Dirichlet and Neumann boundary conditions of our geometry discussed before (*Figure 8b).*

- **Create a mesh.**

Subsequently, we need to create a mesh that generates points in the geometry for which the solution will be calculated. The mesh may be refined as many times as desired, and of course, a deeper refinement will lead to more accurate results. On the contrary, the computational time will obviously be increased. A picture of a mesh refined three times of our example model can be seen in *Figure 8c.*

- **Solve the PDE**

Finally, the PDE may be solved with all the specified conditions. PDE tool also offers the possibility to picture graphically the solution of the gradient in different colors and flow lines to ease the visualization and give an intuitive understanding of the results. (*Figure 8d)*

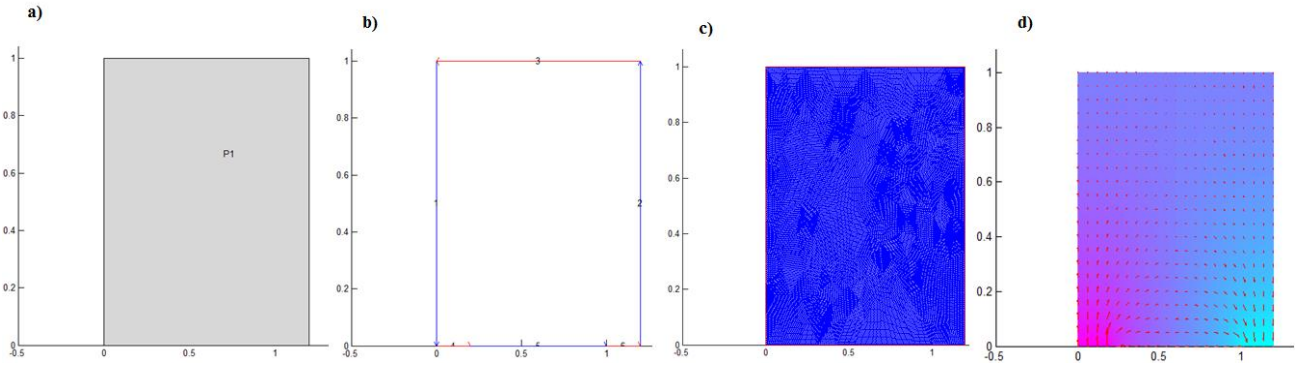

Figure 8. Random geometry drawn in PDE tool **(a).** Specification of Dirichlet BC in red, and Neumann BC in blue **(b).** Mesh creation refined 3 times **(c).** Solution of the PDE and flow pressure gradient lines in the domain **(d).**

3.3.2 Automation of the problem

After understanding the way PDE tool works, we found uncomfortable the required procedure by which the geometry must be created for different problems, as well as the formation of the mesh and the solution of the PDE. Despite the interactivity of the application, it was necessary to automatize the process so that the wanted results could be shown directly, and the program could be easily changed for small alterations in the conditions.

Hence, the next step was to understand the programming behind the application and write a code that would perform the same operations with

common Matlab commands. The program developed for this basic problem should serve as the basis for more complicated approaches. The codes are intended to be open source. In the following section, we describe the code developed step by step.

A basic scheme of how the automation of the application works is shown in the flow chart.

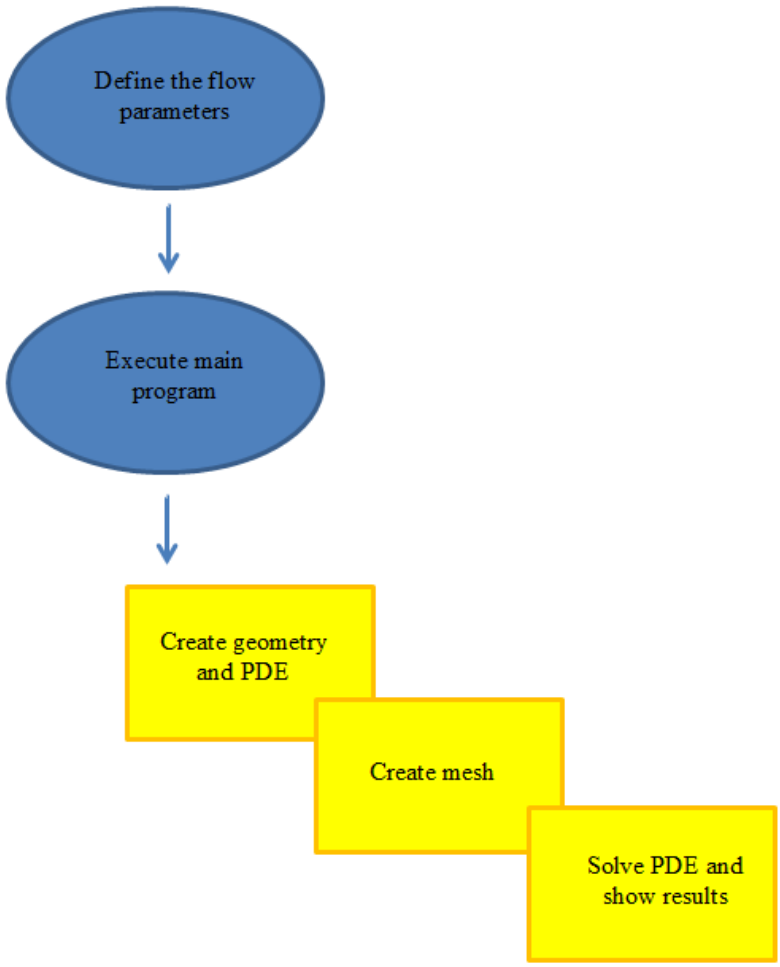

Figure 9. Sketch of the steps followed by the automatized procedure to solve the different models in MATLAB.

In every programming model developed for this project, there is a set of codes that share the same names according to their function in order to ease the utilization by new users that want to make use of the tool. Here, we have a list of them explaining their respective tasks.

1. Flow design

As explained before, the initial step for any model is the description of the parameters of both the geometry and the flow. When executing the different programs, we will always find a file named '*flowdesign'* containing the description of the parameters discussed above, which include those referring to the geometry (H, D, W etc.) and those related to the flow feautures (ρ, μ, Q_0 etc.). These parameters are intended to be changeable according to the user's will. This creates an interactive interface, in which every influence upon features may be tested and analyzed.

2. Solve Device

When executing the program, the next important file that we will find is named '*SolveDevice'* followed by the number of the model we are working with. This code will be the main function by which the rest of the files will be called out. Hereinafter, we discuss the path followed by the program. Any '*SolveDevice'* code will have the typical appearance of the picture shown below.

```
%Solve Device X
clear all
clc

[Pp, Pm, mu, rho, L, D, W, Nc, H, kg, f]=flowdesignX;
PDEsolution
Obtainmesh
```

Figure 10. Generic main function '*SolveDevice'* of a model. It calls the function '*flowdesign*' to establish the parameters of the model, and proceeds to solve the problem.

As we can see, '*SolveDevice'* constitutes the body of the program, and it comprises the different files necessary to solve the target model. In this case, we can check that it starts by executing the function '*flowdesign'* explained before. Once the parameters of the model have been stablished, it executes the next file, named *'PDEsolution'*.

3. PDE solution

'*PDEsolution'* is the name given to the code developed to generate the modeled geometry and the PDE to be solved in it. Hereinafter, we describe the goal of

each command included in the code of the file. The structure of the program '*PDEtool'* is pretty straightforward, and is developed in three well defined steps: creation of the geometry, development of the mesh and assembling of the partial differential equation (PDE).

```
% PDE solution

% CREATE GEOMETRY

geominfo = [2 6 0 0 D/2 W-(D/2) W W H 0 0 0 H]';

geometry = decsg (geominfo, 'Operations', 'Surface names');
```

Figure 11. Geometry description of the first model using MATLAB commands.

To create the geometry, we use the MATLAB command '*decsg'.* This command takes any geometry information stored in a row matrix, and builds up the corresponding geometry according to the instructions given. However, it is not as simple as it seems, and it provides us with a wide range of possibilities to shape any geometry we can think of.

First of all, we need to understand the terminology to describe the wanted geometry. Any 2D domain will be described into a geometry description matrix (GD). The structure of the description matrix will vary depending on the geometry described. The first row indicates the type of geometry (1 for a circle, 2 for a polygon, 3 for a rectangle, and 4 for an ellipse). The rest of the indicators for each different domain are described below:

Circle: gd = [1 center(x) center(y) radius]

Polygon: gd = [2 #lineSegments x_1 x_2 x_{3etc} y_1 y_2 y_{3etc}]

Rectangle: gd = [3 polygonformat]

Ellipse: gd = [4 center(x) center(y) $semiaxis_1$ $semiaxis_2$ rotationalAngle]

In MATLAB, the command *DL = decsg (GD, SF, NS)* decomposes the solid objects described by the geometry description matrix (GD) into the minimal regions (DL) represented by the decomposed geometry matrix. (NS) just contains the names of the different geometry matrixes, and (SF) is the operating formula that needs to be performed with the different geometries.

In simple words, we will define the different geometries that will compose our problem, and then perform addition / subtraction operations to end up with the seek geometry. Below, we show an example of how to build a geometry described by a square with a circular hole in the middle:

```
%CREATE GEOMETRY

geominfo=[3 4 0 0 1 1 0 1 1 0;
    1 0.5 0.5 0.25 0 0 0 0 0 0;]';

geometry = decsg (geominfo, 'SQ-CR',
    [('SQ')' ('CR')']);

pdegplot(geometry)
title('Square - Circle')
```

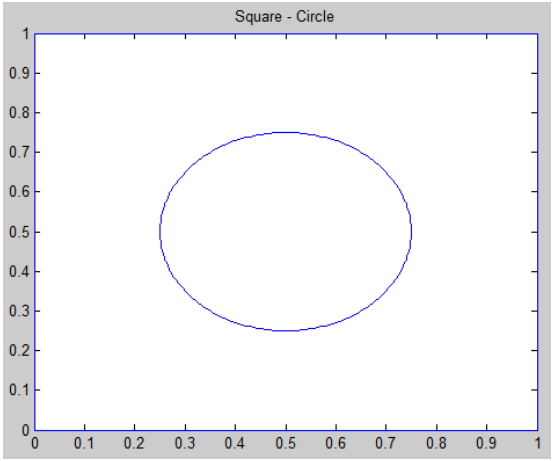

Figure 12. Example of the construction of a 2D domain by subtraction of figures using '*decsg*'.

The next step is to create the mesh. As we have herein discussed, the mesh is a set of arbitrary points that divide the geometry of our problem for further analysis. The solution to the PDE will be calculated in those points. Naturally, the separation between each point may be chosen as small as desired by refining the mesh as much as wanted. Of course, a deeper refinement will result into more accurate results, since the solution will be calculated in an ideally continuous medium, instead of a discrete set of points. However, as it is also logical, a higher refinement also results in an increased computational time.

Figure 13 shows the code that converts our geometry into a mesh of triangles:

```
%CREATE MESH

[p,e,t] = initmesh(geometry);

%refine mesh NR times

NR = N;
for i = 1:NR
    [p,e,t]=refinemesh(geometry,p,e,t);
end

Jiggle Mesh
```

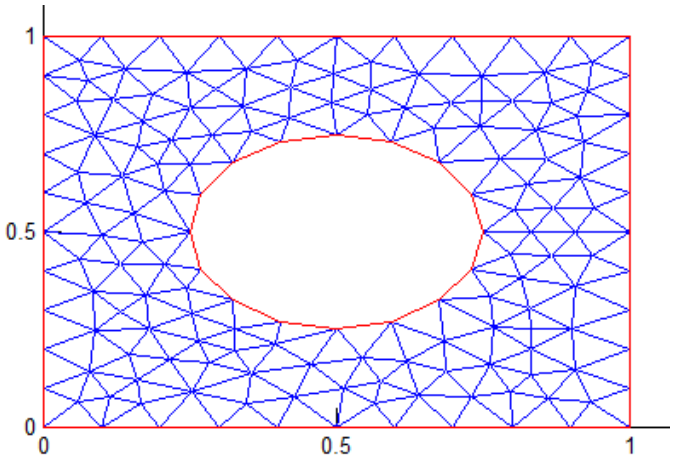

Figure 13. Code to develop a mesh in the geometry, and visual result of the mesh in the geometry.

In the following image, the progressive change in the mesh as the refinement is increased can be appreciated *(Figure 14).*

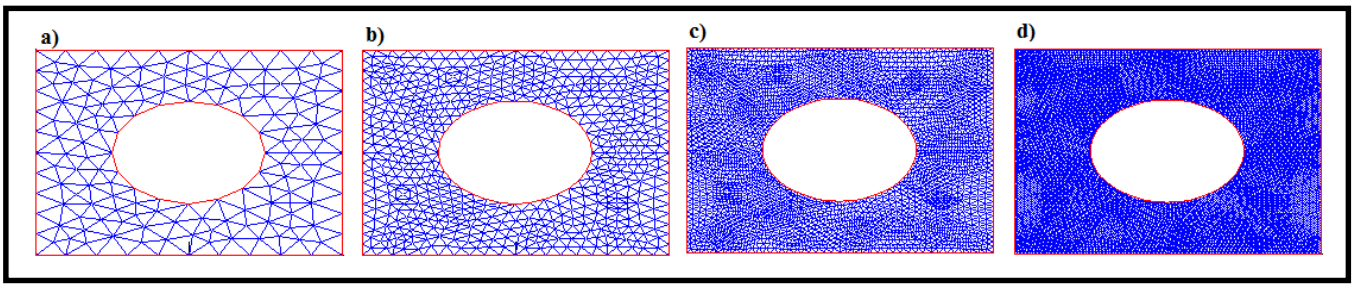

Figure 14. Visual progression of the mesh as the number or refinements increase, one (a), two (b) and three refinements (c).

Once the geometry on which the problem will be solved has been created, we proceed to apply the PDE we need to solve. In this case, as we have deeply examined before, the PDE that applies corresponds to the Laplace's equation, which is nothing else but a special case of the electrostatic equation.

Matlab's distinctive command to assemble PDEs on a target geometry is called '*assempde',* and has the following form: U = assempde (B,P,E,T,C,A,F).
ASSEMPDE assembles and solves the PDE problem stated by the general formula:

$$-\nabla\,(c * \nabla\cdot(u)) + a*u = f$$

This formula represents the general form of a partial differential equation. The diverse types of PDEs originate by giving different values to the inside parameters. In our case, the Laplace equation goes as follows:

$$-\nabla\,(1 * \nabla\cdot(u)) = 0$$

Being c = 1, a = 0, and f = 0.

P, E, T are the data describing the mesh of our geometry, and B is a file specifying the boundary conditions of our problem. Therefore, we need to explain the method to stipulate the BC before we can continue.

- **Boundary conditions**

The process to determine the boundary conditions of a problem in a given geometry is always similar. First of all, we need to know the *label* of the edges. When we create a geometry as we have explained here, Matlab assigns a

certain number to each edge composing the problem, usually based on their length. The *label* given to each edge can be easily known by plotting the geometry once it has been created:

```
%pdegplot(g,'edgeLabels','on');
```

We have defined the different types of Boundary Conditions, existing two main classes: Dirichlet and Neuman. It is worth to know that Matlab assigns Neumann conditions to every boundary by default, so we just need to postulate those that refer to the boundaries with Dirichlet BC. The method was learnt from an example provided by MatlabWorks

After this parenthesis referred to the Boundary Conditions, we may well advance in the problem of the PDE solution. As we have concluded, at this point we have our geometry divided into a mesh of triangles for which the solution to the pressure field at each point has been calculated. *Figure 15* shows the result of the plot of the pressure field solution for our first model. As we can check, the contour lines for equal pressure distributions are included in the picture.

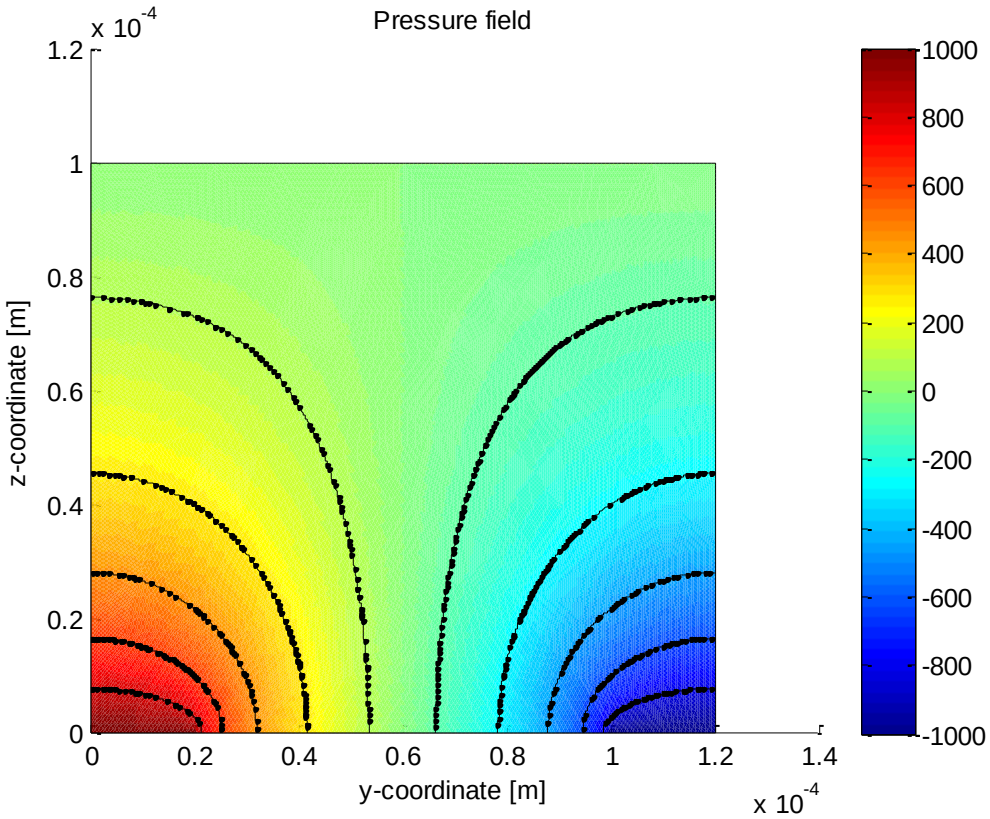

Figure 15. Visual solution to the pressure field in the Domain. The channels' pressures appear in the bottom left corner (Positive channel) in red, and bottom right corner (Negative channel) in blue. The upper boundary represents the top of the fibrin gel open to the atmosphere, P = 0.

So what is next? We must not forget that the goal of our problem is linked to the generated flow between channels, not the pressure field, although they are greatly related. With the purpose of understanding their relation, we will apply to the Darcy's law, which describes the flow of a fluid through a porous medium. Darcy's law may be derived from the Navier-Stokes equation.

The law states that the total flow (Q) through a porous medium is equal to the ratio between the permeability of the medium (k) times the cross-sectional area to the flow (A) times the pressure drop (ΔP) and the viscosity of the fluid (μ) times the length (L) taken into account.

$$Q = -\frac{KA}{\mu}\frac{\Delta P}{L}$$

- **K** is the characteristic permeability of the medium
- **A** is the cross-sectional area of the channel
- **μ** is the dynamic viscosity of the fluid [N·s/m^2]
- **ΔP** is the pressure drop along L [Pa]
- **L** is a characteristic linear dimension, (travelled length of the fluid) [m]

* The minus sign in the equation is necessary since the flow always goes from high-pressure to low-pressure areas.

Dividing both sides of the equation by the area, and considering infinitesimals steps in the longitudinal direction, we get the value of the flux (flow per unit area) [m/s].

$$q = -\frac{K}{\mu}\nabla P$$

- **q** is the flux [m/s]
- **K** is the characteristic permeability of the medium
- **μ** is the dynamic viscosity of the fluid [N·s/m^2]
- **∇P** is the pressure gradient [Pa/m]

Strictly speaking, this value of the flux is not the actual velocity of the moving fluid, even though they share units. This is due to the fact that the medium is porous, and it has a certain influence in the velocity of a hypothetical object travelling within the fluid (v = q / ϕ; ϕ = Porosity). However, having this misconception in mind, we will call this factor *'velocity'* in the next pages.

Using some Matlab commands we can calculate the pressure gradients from the pressure field obtained after solving the PDE, and from then, we are able to compute the velocities at each point. Now that we have the velocities, we just need to integrate the target regions of our geometry to get the flow. In our case, we are interested in the outcoming / incoming flow of the positive and negative channels, and the possible flow loss on the upper boundary (where the keratinocytes will develop).

The solution to the velocity field can also be plotted *(Figure 16).*

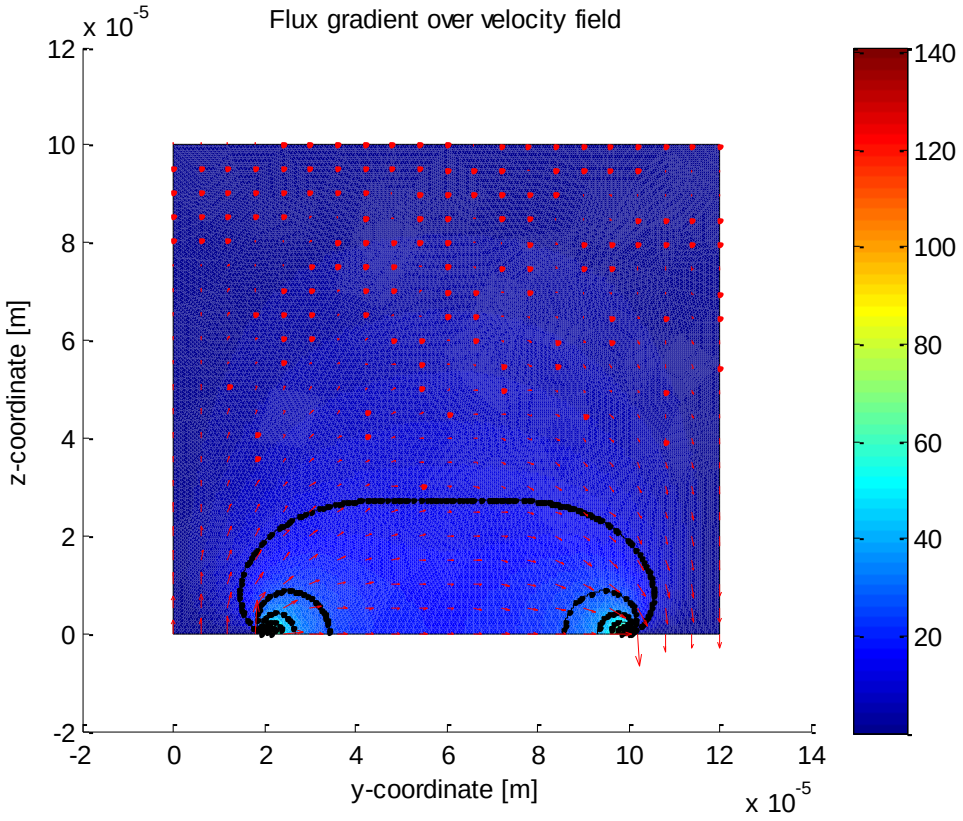

Figure 16. Plot of the velocity field in the 2D domain of the model. Velocity flux direction is depicted by red arrows.

The integration was performed using *Trapezoidal Numerical Integration* (trapz). We are interested in the flow rate, for instance, that escapes the positive channel. With the program beforehand described, we were able to compute the velocities of the flux in the channel's boundary. Now we need to integrate the velocity profile, since Q = $\int \vec{v}\, db$, where '*b*' refers to the boundary. The method of integration used was the trapezoidal rule. The trapezoidal rule works by approximating the region behind a function f(x) as a trapezoid and calculating the area. The resolution (spacing between trapezoids) was set equal to the

distance between the points of the mesh. *Figure 18* shows how the trapezoidal rule approximates the integral of the function *f(x).*

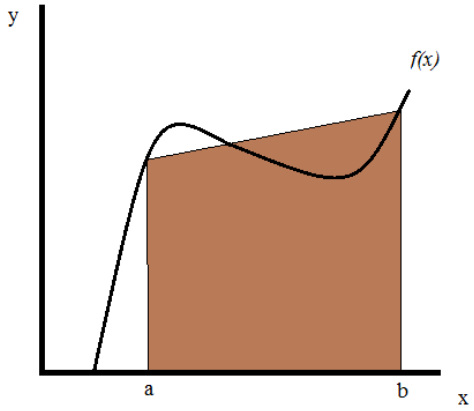

Figure 18. Example of an approximation to the integral of *f(x)* by the trapezoidal rule in the interval (a,b).

3.3.3 Analysis of the model

The code we have developed will now be able to calculate the pressure field over the depicted geometry, then to simulate the flux over the gel, and finally to evaluate the flow rate that escapes one channel and goes into the other.

The model that we have conceptualized aims to simulate the skin construction, being composed by a permeable fibrin gel, which would simulate the dermis, and a set of well-structured channels that mimic the blood vessels of the organ. This model serves as a basis for the development of any other possible approach we may think of. In this case, we decided to place the channels under the gel, and allow for diffusion in just one direction. However, this tool permits the evaluation of different geometries and locations. *Figure 19* shows different models that can be developed modifying the conditions of the model.

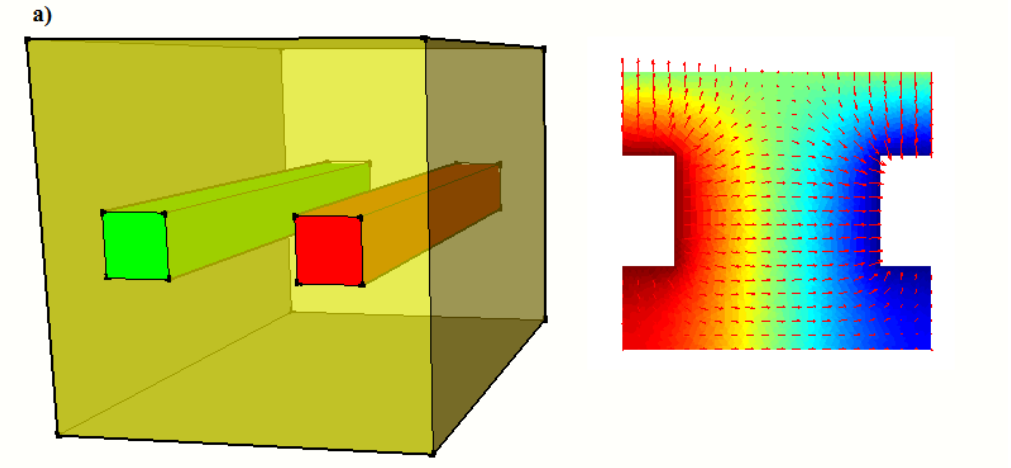

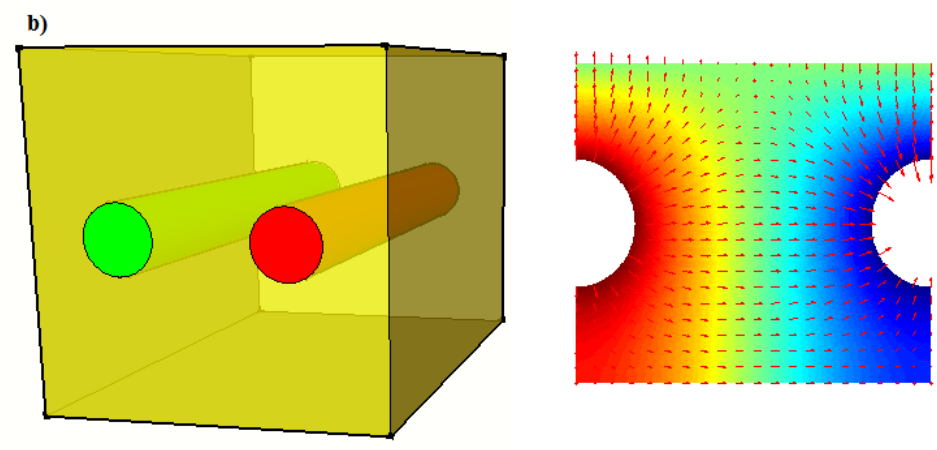

Figure 19. Example of two possible models with squared (a) and circular (b) cross-section channels positioned in the middle of the gel.

However, despite the apparent power of the tool, there are some constraints that must be analyzed. In this section, we describe a set of limitations posed by this simple approximation, which could be straightforwardly solved by changing some of the characteristics of our device.

Regarding the transversal direction, the main restriction of the model would be the limited height that the flow reaches, which would have a high influence on the thickness of the skin. Even though the thickness of the gel may be designed as wanted, the velocities will decrease exponentially as we estrange from the channels, and as a consequence there will always be a maximum distance traversed by the fluid. This fact strictly defines a limit in the potential thickness of the culture, which could be lower than necessary. In fact, the trials with this model did never exceed a thickness of 600 µm in height, whereas the mean length of human fibroblasts AGO 1523 is around 200 µm.

This constraint may be easily overcome by developing a model with several layers, in which the channels are engraved inside the gel. This way, the available culturing region would be indefinitely increased. Once again, the geometry as well as the placement of the channels may be engineered in different ways, and differences in efficiency may be evaluated. It must be taken into account, that the programming of the model requires only the basic symmetry among the channels. The expansion of the dimensions is a mere fabrication issue.

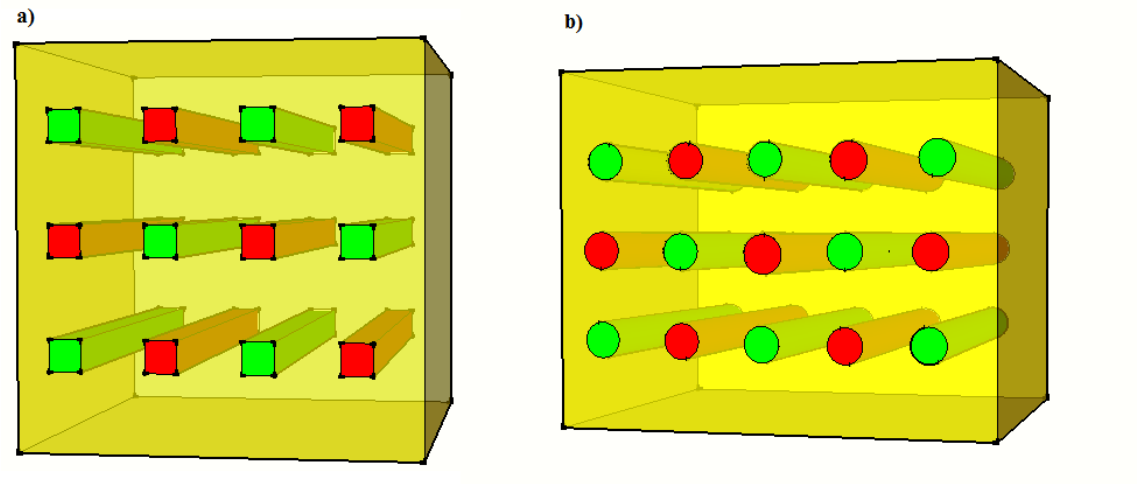

Figure 20. Graphic representation of multilayered, squared (a) and circular (b) cross-sectional channels models.

However, it is regarding the longitudinal direction where we find trouble. One of the most important points in the design of this 'organ-on-a-chip' is the amount of nutrients that reaches the cells throughout the fibrin matrix. The flux that transverses the channels is motored by the pressure difference between them, as it has been discussed. However, as fluid exits the positive channel and enters the negative one, the pressure in the former decreases to foster an increase in the latter. This drop in the channel pressure difference along the longitudinal direction will result in a reduction of flux across the gel as we advance forward until pressures stabilize, where no flux would occur. The alteration of the flux, and consequently of the nutrient supply at the different regions of the device could be dramatic for the culture integrity. It could greatly restrict the available culture region in this direction.

We must evaluate this important imperfection of the model that could affect the efficacy of our device.

3.4 Improved model

In this section, we will describe a new model that takes care of the difficulties previously described.

As we have discussed, the main goal of the project is to design a microfluidic chamber that furnishes the cells intrinsic to a fibrin matrix. Therefore, we wish to develop a culture that can be extended as much as desired in all directions, keeping a constant nourishment supply ubiquitously. The main objective of this model is to overcome the problem of the pressure loss along the channels, with

the purpose of maintaining a stable flux of fluid across the fibrin gel. To do so, we have designed a new approach wherein the area of the channels is varied in the longitudinal direction in order to be able to counteract the effect that the fluid loss originates in the pressure difference amongst the channels.

The appearance of this design is shown in *Figure 21.* The picture shows how the area of the positive channel would decrease in a constant fashion according to the flow rate loss, whereas the negative channel's cross-section increases inversely.

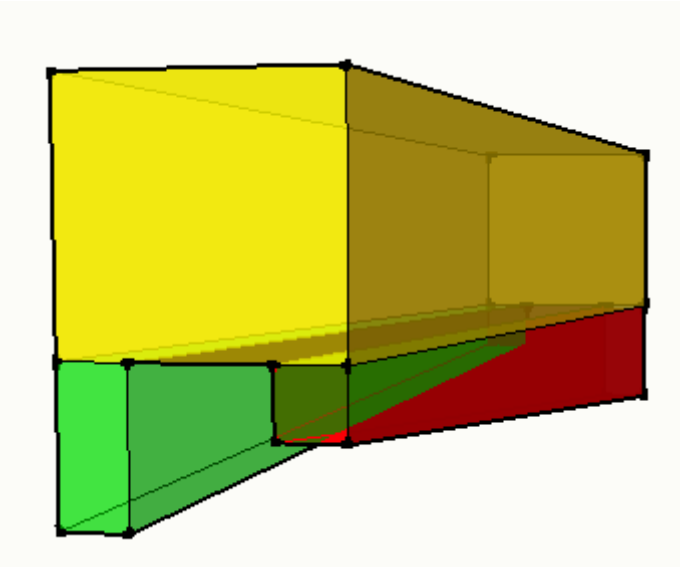

Figure 21. Simulation of the improved model with varying cross-sectional area channels.

In order to solve the problem, we developed a new program dealing with the necessary changes to simulate the model. As in the first approach, in a first attempt we will describe a simplified model in which the channels do not form part of the permeable gel, but are situated in a solid layer under it. Nevertheless, the code may be adapted to account for the complex device, where the fluid escapes the channels through all the walls. As before, the flux will travel from one to the other due to the pressure difference between both.

3.4.1 Automation of the problem

The automation of the problem will have the same structure as in the first approach regarding the initial step.

The difference will arise from the calculation of the pressure drop along the channels. Therefore, specific formulae for this problem must be modified.

The problem is characterized by a flow along the channels due to a constant pressure gradient (Pp, Pm) that causes the motion of the fluid from high to low pressure regions. The width of the channels will remain constant (D), but their heights (Hp and Hm respectively) will vary as described. *Figure 22* shows the control surface of the initial step of the problem.

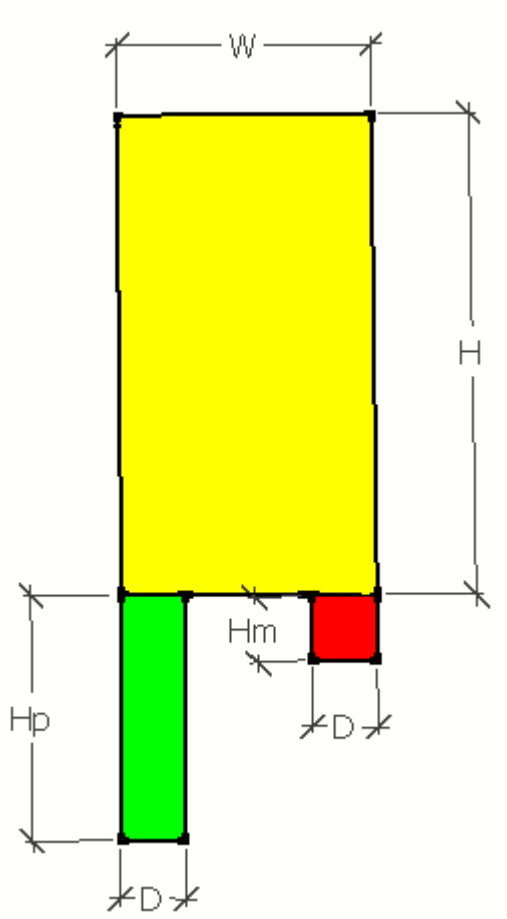

Figure 22. 2D domain of the model, with descriptive dimensions of the device's parameters.

In order to build the equations that describe our model, we are going to treat this problem with the description of the *quasisteady viscous flow in a channel of slowly varying region.*

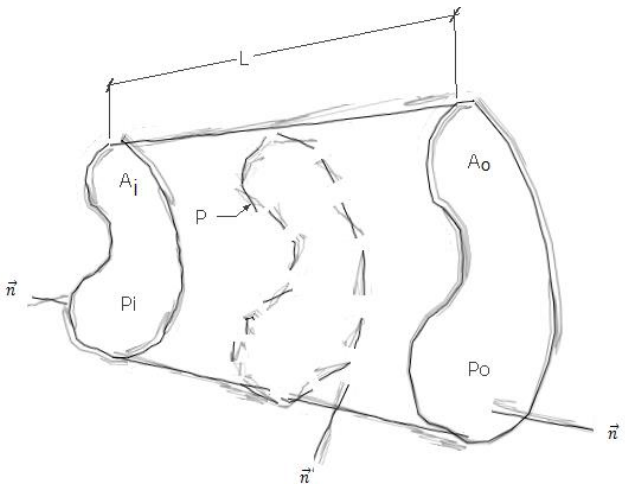

Figure 23. Arbitrary control volume of a channel of length L, cross-sectional area variation Ai - Ao, and pressure difference of Pi – Po between both ends.

In the problem, momentum conservation can be applied. The motion is the result of the pressure gradient along with the friction with the surrounding walls associated with viscous forces. The momentum conservation equation is,

$$\int_{\Sigma c} \vec{\rho}\, \vec{v}(\vec{v} \cdot \vec{n})\delta\sigma = -\int_{\Sigma c} P\, \vec{n}\, \delta\sigma + \int_{\Sigma c} \bar{\bar{\tau}} \cdot \vec{n}\, \delta\sigma$$

where $(\vec{\rho}\, \vec{v})$ refers to the linear momentum per unit volume, and $(\vec{v} \cdot \vec{n})\delta\sigma$ is the volume per unit time that crosses the surface. Since the control volume is stationary, the amount of fluid that enters the volume is the same amount that exits it, and hence, the first term of the equation is zero.

$$0 = -\int_{\Sigma i+\Sigma o+\Sigma w} P\, \vec{n}\, \delta\sigma + \int_{\Sigma i+\Sigma o+\Sigma w} \bar{\bar{\tau}} \cdot \vec{n}\, \delta\sigma$$

Then, we have to evaluate the integrals of the pressure gradient and viscous forces on the surface involving the control volume (the inlet, outlet and walls). As shown in the descriptive image, the pressure gradient affects to the inlet and outlet cross sections. It is important to take into account the direction of the normal vector to the surfaces, and its sign. Regarding to the viscous forces that originate from the friction between the fluid and the walls, in the direction opposite to the flow, we need to assume the hypothesis that it is constant all along the volume.

$$0 = -Pi(-\overrightarrow{ex})\mathrm{A} - \mathrm{Po}\,\overrightarrow{ex}\,\mathrm{A} - \tau\mathrm{w}\,\overrightarrow{ex}\,\mathrm{PL}$$

Now, we need to introduce the concept of hydraulic diameter. The hydraulic diameter (Dh) is a commonly used term when dealing with a flow in a non-circular channel. The hydraulic diameter of a pipe of random geometry is defined as (Dh = 4A/P), which corresponds to the diameter of a circular pipe, if we substitute by the appropriate values of the area (A= πR^2) and the perimeter (P=2πR). From the above equation we come up with the following expression:

$$\tau_W = \frac{Pi - Po}{L}\frac{A}{P} = \frac{\Delta P}{4L} Dh$$

Also, the viscous forces in a pipe are calculated by definition:

$\tau w = \frac{\rho v^2 f}{8}$, where (*f*) is the friction factor. This is calculated experimentally for different geometries, and must be looked up in each independent case. Equating the two expressions we end up with the following formula for the pressure drop along the channels:

$$dPdx = \frac{1}{2}\frac{\rho v^2 f}{Dh}$$

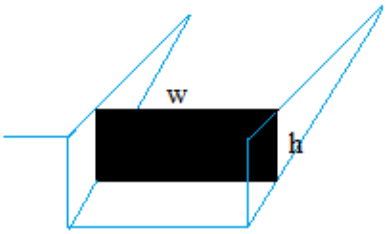

$$Dh = \frac{2wh}{(w+h)}$$

Relating the mean velocity with the flow rate (v = Q/A), we get the expression for the pressure variation.

As we can see, this brings us to a new system of differential equations that describe the model. In this case, there are six equations that are interrelated amongst them by the pressure and flow rate.

(4) $\frac{dP+}{dx} = -\frac{1}{2}\frac{\rho v^2 f}{Dh}$

(1) $\frac{dQ-}{dx} = \frac{D\bar{K}}{\mu W}\Delta P$

(5) $\frac{dP-}{dx} = \frac{1}{2}\frac{\rho v^2 f}{Dh}$

(2) $\frac{dH+}{dx} = Hpo - mx$

(6) $\frac{dQ+}{dx} = -\frac{D\bar{K}}{\mu W}\Delta P$

(3) $\frac{dH-}{dx} = Hno + mx$

Figure 24. Variations of the positive (1) and negative (2) pressures along the longitudinal direction, and the flow rate and height of the positive (3) , (5) and negative (4), (6) channels.

Once again, the values of the flow rate losses (dQp/dx) and (dQm/dx) will be calculated numerically.

3.4.2 Longitudinal integration

As repeatedly remarked in the project, the solution to the models implies two main parts; on the one hand, the analysis of the flux behavior at any slice of the plane (y-z) of the device, on the other hand, the prediction of the flow progress along the longitudinal direction. Regarding this new approach, firstly, the analysis of the 2D varying-cross-section domain will be performed by the program described for the basic model with the necessary variations for the adaptation to the new approach. Secondly, the solution concerning the longitudinal problem will be done using looped programming.

To address the problem, we will use ODE 45 tool provided by Matlab, which is aimed to solve nonstiff differential equations by numerical methods. The ODE 45 function requires three inputs that correspond to the ODE function to be solved, the solution interval, and the initial conditions.

ODE45 (@odeFunction, tspan, Xo)

This function will be used to solve the variation of the six unknowns (P_+,P_-,Q_+,Q_-, H_+ and H_-) along the longitudinal direction given the initial conditions.

The equations of the parameters were analytically developed, and shown in *Figure 24*. However, the non-constant $\bar{k}$ factor that relates the flow rate loss (dQ/dx) with the pressure-difference between channels should be obtained mathematically. With this factor, we could use ODE45 to solve the six equations from their mathematical expressions. Nonetheless, we may resolve this problem by calculating the value of dQ/dx numerically.

The goal is to perform looped programming so that the pressure variations calculated at one point dx will be the flow parameters for our program to calculate the flow variations at that slice. These variations will be used to compute the next pressure variation at a new slice separated by dx from the previous one. The process will be repeated for a distance x = L, where L is the length of the channels in our device.

3.3. Microfabrication of the device

This project is based on the development of a microfluidic chamber to culture skin in vitro. Inside the field of study of biological microdevices, or BioMEMS (Biomedical Micro-Electro-Mechanical System), it could be classified into the well-known '*Lab on a Chip'* (LOC) type, which is concerned with the miniaturization and integration of laboratory processes into single chips that often involve microfluidics.

Microfluidics is the multidisciplinary field involving engineering, physics, chemistry or biotechnology among others that focuses on the design of systems in which very small volumes will be handled with a practical application purpose.

In this document, we have described and analyzed two different models that have diverse expediencies: the '*single dermis-layer model'* and the '3D *skin-on-a-chip model'*. Several microfabrication techniques, together with the procedure to manufacture the device in its final form, as well as the culturing process, are herewith discussed.

- Single dermis layer model

The first model analyzed in this project refers to the combination of a single-layer of microfabricated channels integrated into an impermeable structure in direct contact with a permeable gel that allows for fluid diffusion. Even though this approach is not enough for the development of a complete 3D skin's structure due to the thickness limitation of the permeable gel, it could serve to improve the current processes of single-layer cell culturing.

The process by which skin is currently grown in the lab is highly product-consuming. When there is a need for a skin transplant, a 1 cm^2 sample of the epidermal cells from the patient is harvested and extended to the desired size to cover, for instance a burnt wound. In the lab, a monolayer of keratinocytes is grown by placing the sample in a petri dish and immersing the cells of a culture media, which contains the necessary growth factors and nutrients for their growth and division. Later, this monolayer is directly placed over the wound, and is immediately vascularized and incorporated in the patient's body. This is a simple protocol that follows an every-day used technique that is mastered by scientists in the lab. However, there is a waste of expensive products in every culture that could be avoided if the cells were grown with the appropriate medium amount at its final concentration of products.

The first approach of our model could be used as a basis for fluid supply to any type of cell culture. As a consequence of the limited possible height, the device

would pose difficulties to grow fibroblasts within the fibrin gel. Yet, the model could be used as a supply method to nourish any type of cell cultured on top of the gel. In fact, it would not be even necessary to use fibrin, but the model could be customized by the utilization of any other biocompatible, permeable gel, such as PDMS.

In order to microfabricate the gel with the desired geometry, we could follow several approaches. One of them would be direct patterning of the gel already constructed. Another one would be the development of molds of appropriate dimensions. These molds could be made with different materials, and any microfabrication technique providing the necessary resolution could be used, such as 3D printing, photolithography, micromolding etc. A graphical simulation of the mold on which the gel could be developed is shown in *Figure 25*.

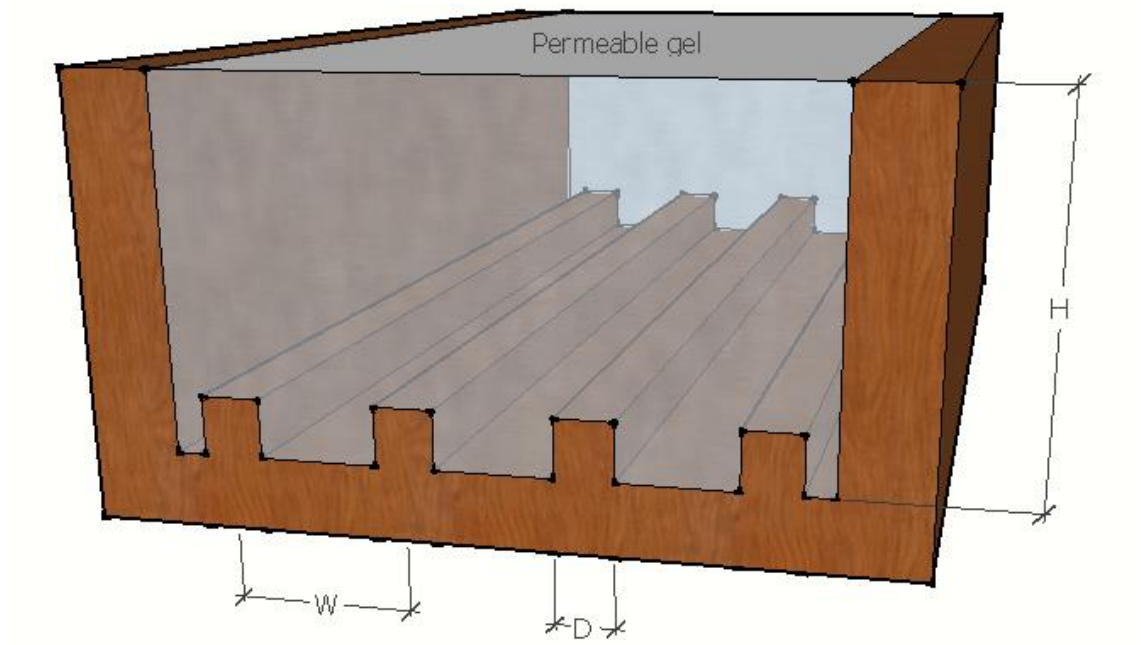

Figure 25. Sketch of a microfabricated mold for gel development.

Afterwards, the permeable gel would be inserted in another device able to connect micropumps to the channels. This way the single-layered culture could be carried out on top of the gel. The design of the pumping method should carefully be studied, such as the number of micropumps, (one per channel /one for every channel with the same pressure), the location of the micropumps (on the same side / opposite sides of the device), the motion of the fluid (all in the same direction / positive channels in one direction and negative ones in the opposite direction) etc. A simplistic simulation of the final appearance of the device is shown in the next figure.

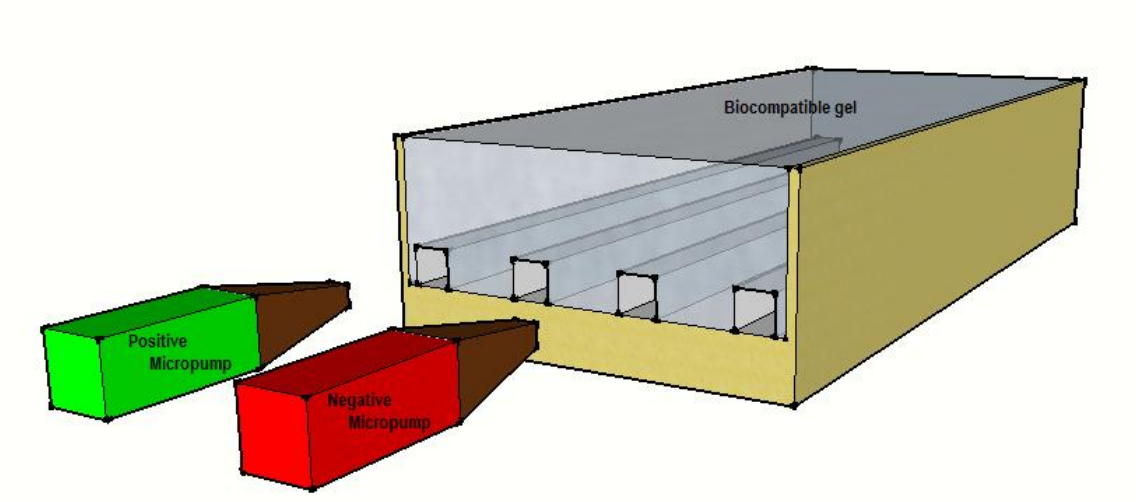

Figure 26. Graphical simulation of the microfabricated device to grow a single-layer of cells on top of a biocompatible, permeable gel.

- Skin-on-a-chip

Fabrication process:

In this section, we describe the protocol that should be implemented in order to grow a differentiated skin in vitro that follows the model herein described. This more complex approach is intended to be able to grow and reproduce a whole 3D skin tissue in its natural behavior.

The design of the mold could be the same as the one described before. However, there would be a need to develop a protocol to be able to assemble the fibrin gels one on top of the other, since this model is based on multilayered channel sets to avoid height restrictions. Nevertheless, we must not forget that any procedure that results in the microfabrication of the final geometry would be valid. For instance, the structure of the gel without the channels could be built, and later micropattern the channels using laser ablation techniques In any case, the best method to fabricate the device is out of the scope of this project, and should be studied in depth.

In what follows, we will define the process by which the fibrin gel would have to be developed:

- First, the blood plasma should be isolated by centrifugation. A chelating agent should be added to the Calcium in blood, to avoid coagulation of the plasma in contact with the air.

- Then, the fibroblasts should be isolated to the final dermis concentration. Due to the diverse composition of the dermis, (which contains elastin, fibrin, ECM etc.) the composition of the ECM is extremely important for the fibroblasts development.

- Next, the fibrin gel must be prepared at a known final fibrin concentration. This is important, since it will determine the permeability of the resultant gel, as well as the pore size that will regulate the diffusion of nutrients. (22)

- Finally, we would mix our cells with the fibrin, and pour the mixture on the microfabricated mold. Solidification of the plasma will be caused by addition of an excess of Ca, or thrombin if necessary.(23)

We will obtain a permeable fibrin gel populated by fibroblasts, with hollow channels engraved through which the nutrients will be supplied.

In an ideal model, the channels could be cellularized with endothelial cells by addition of vascular growth factor that promotes vasculogenesis, creating real blood vessels within the fibrin gel.

4. RESULTS AND DISCUSSION

4. Results and Discussion

After discussing and comprehending the power of the tool, it is time to get some insightful information about the model. In this section, we will display and analyze some of the results that can be extracted from the different approaches.

4.1. First Model

First of all, we need to set the standard value of the parameters implicated in the results. The final estimation of these values was done taking into account physical fabrication restrictions, and especially physiological information about the natural skin derived from the literature, as it has been discussed in previous sections.

Although the solution to the problem in the model will always have a similar illustrative pattern, it is important to have in mind that any little variation in the conditions of the problem will lead to different numerical results. Henceforth, the influence of every parameter was tested to decipher their importance in the design. According to these statements, the standard values given to the different factors are:

Default Parameters	
Pressure difference between channels **(ΔP)**	2000 [Pa]
Pressure on the top of the gel **(P)**	0
Thickness of the gel **(H)**	300 [µm]
Separation between channels **(W)**	400 [µm]
Side of the square channel **(D)**	200 [µm]
Viscosity of the fluid **(µ)**	0.8 e-3 [kg/m.s]
Density of the fluid **(ρ)**	1000 [kg/m^3]
Permeability of the gel **(k)**	1e-15 [m^2]
Initial flow rate **(Qo)**	2.5e-11 [m^3/s]
Length of the device **(L)**	10e-2 [m]
Number of mesh refinements **(NR)**	5

Repeated simulations of the model design were done with the intention of working out the configuration of values of the parameters that yield the desired flow behavior in the model. Regarding the structural parameters, a final channel width of D = 200 µm was chosen. This value of the channel's cross-sectional side has an important influence in the Reynolds number of the model as well as

in the pressure drop along the channels. Consequently, the distance between the center of the channels was set to W = 400 μm, and the total thickness of the gel was chosen to be H = 300 μm, even though the influence of the later on the flow comportment is less significant. Likewise, the total length of the design was maintained at L = 1 cm, which should satisfy the conditions for the functionality of the microchip. The dimensions of these parameters lead to a proper flow design, while easing the microfabrication process of the device. Besides, the pressure difference between the channels was set to ΔP = 2000 Pa in the simulations. However, this value may be straightforwardly modified to obtain an appropriate flow rate throughout the gel without altering the proper workability of the model, as long as it does not risk the integrity of the structural components of the approach. A value of Qo = 2.5e-11 m^3/s, (0.025 μl/s) was chosen for the initial flow rate in the channels. This value of the flow rate derives into a mean velocity v = 6.5e-4 m/s, which corresponds to the physiological velocity of the blood into the capillaries, as documented in *section 3.2.2*. Finally, the permeability of the gel had to be decreased by several orders of magnitude to avoid excessive flow loss through the channels. This fact may be explained by the existence of the endothelium in veins and arteries that serves as a physical barrier between the blood inside the vessels and the fibrin matrix that forms the dermis. This cell-layer most definitely lowers the diffusivity of nutrients outside of the blood, resulting into reduced flow diffusion.

One of the most important aspects of the parameter's configuration is to ensure that the initial hypotheses of the flow behavior inside the channels are fulfilled: laminar behavior of the flow and slenderness. These assumptions will apply for fluids with Reynold's number close to zero.

$$Re = \frac{(\rho * v * D)}{\mu} = 0.1629$$

Hereinafter, the influence of each parameter in our model will be examined.

First of all, we tested the successful functioning of the program. As discussed in this document, we are interested in the final result of the flow field in the specified geometry. Plotting the results obtained, and patterning the flux with velocity arrows, we get the following outcome:

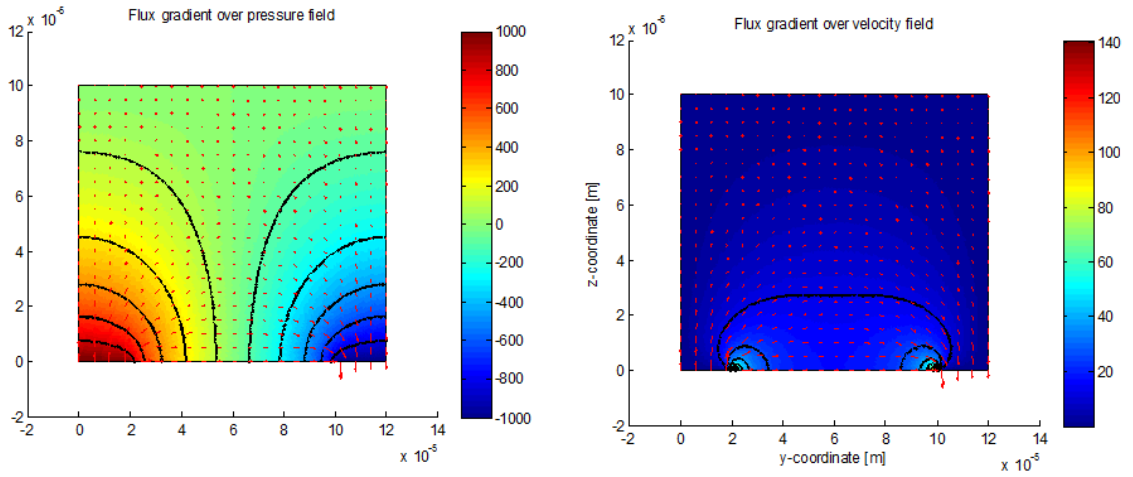

Figure 27. Graphs of the pressure field and velocity profile, and contour lines results with the given initial conditions.

The tool developed calculates the flow loss from the positive channel by numerical integration of the velocity flux for a certain geometry given the defining parameters of the problem. One of the requirements for the program to be considered successful is to ensure that the amount of fluid within the system is kept constant, that means, that the integration of the amount of fluid that enters / escapes the positive channel plus the amount of fluid that enters / escapes the negative channel plus the amount of fluid that enters / escapes the top boundary equals zero, giving a negative sign to the fluid escaping a surface and a positive sign if it enters the surface for convenience. The following expression was used to assess the error percentage of the calculations:

$$dQdxError\ (\%) = \frac{abs(dQpdx + dQndx + dQroofdx)}{dQpdx} * 100$$

Where $dQpdx$ refers to the flux out of the positive cannel, $dQndx$ represents the flow rate into the negative channel, and $dQroofdx$ denotes the flux at the top boundary.

A different way to calculate the error of the program is to make use of the analytical expression of the flow rate variation:

$$dQpdx = \frac{DK}{\mu W}\Delta P$$

From this expression, the value of the (K) factor can be figured out from the expression, having calculated $dQpdx$ numerically. The analytical expressions that describe the flow were presented in *Figure 24*. A prompt understanding of the accuracy of the numerical method is obtained by direct comparison with the permeability factor established in the flow design. Then, the expression of the error will be derived by comparing the (k) value obtained from the analytical expressions of $dQpdx$ and $dQndx$.

$$Kerror(\%) = \frac{abs(Kpositive - Knegative)}{Kaverage} * 100$$

$$Kpositive = \frac{-\mathrm{dQpdx} * \mathrm{W} * \mu}{\mathrm{D} * \Delta\mathrm{P}}$$

$$Knegative = \frac{\mathrm{dQndx} * \mathrm{W} * \mu}{\mathrm{D} * \Delta\mathrm{P}}$$

$$\mathrm{Kaverage} = \frac{\mathrm{Kpositive} + \mathrm{Knegative}}{2} * 100$$

The following table shows the results of these expressions for the given standard values of the parameters.

$dQpdx$	$dQndx$	$dQroofdx$	Error ($dQdx$)
-7.133e-14	7.096e-14	-4.1465e-18	0.519%

K	*K*positive	*K*negative	Error (*K*)
6e-20	5.6907e-20	5.6614e-20	0.515%

As we can check, the error of the program is minimal. In fact, we may plot the integrands that lead to the flow rate at the boundaries, which are the velocity profiles at the channels and roof boundaries. The following figure shows the appearance of these integrands, that show high symmetry as it can be

observed. The interchange of flux through the top boundary would be related to the amount of fluid reaching the keratinocytes on the gel.

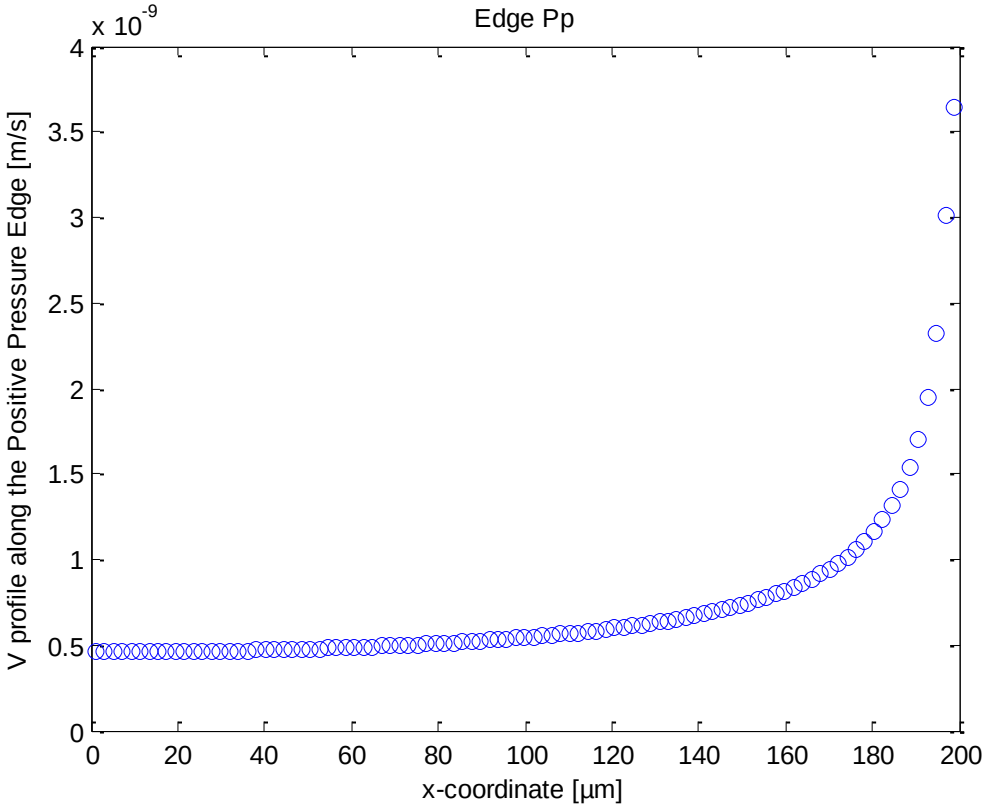

Figure 28. Velocity profile (integrand of the flow rate) at the positive channel boundary. It represents the velocities at which the fluid is escaping the channel.

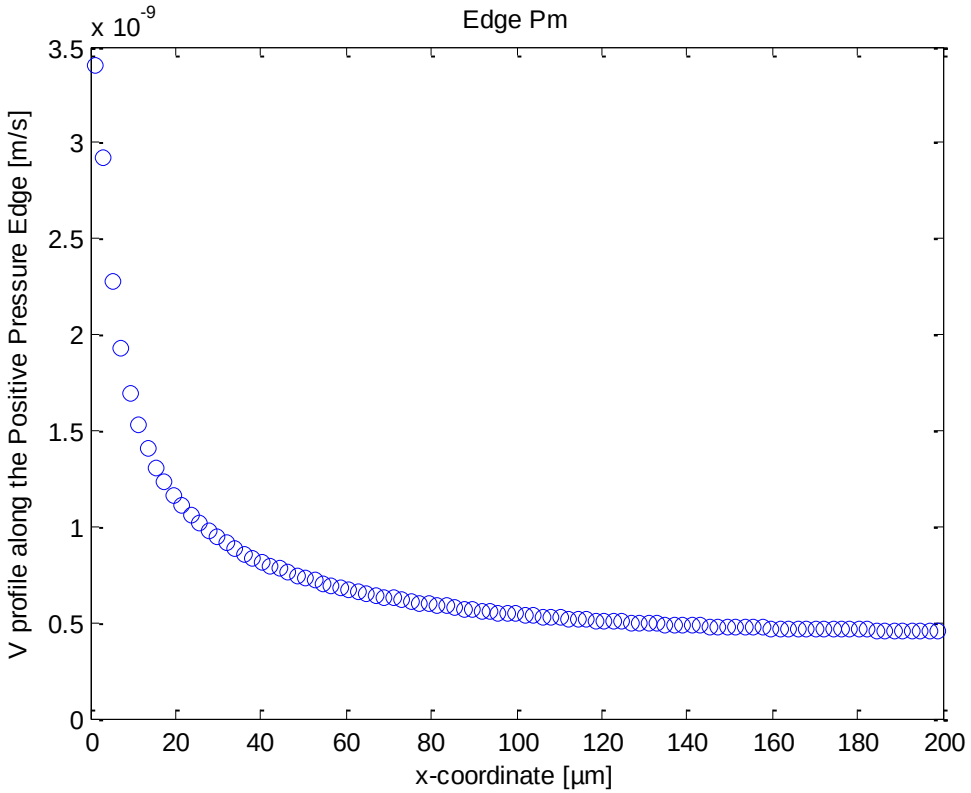

Figure 29. Velocity profile (integrand of the flow rate) at the negative channel boundary. It represents the velocities at which the fluid is entering the channel.

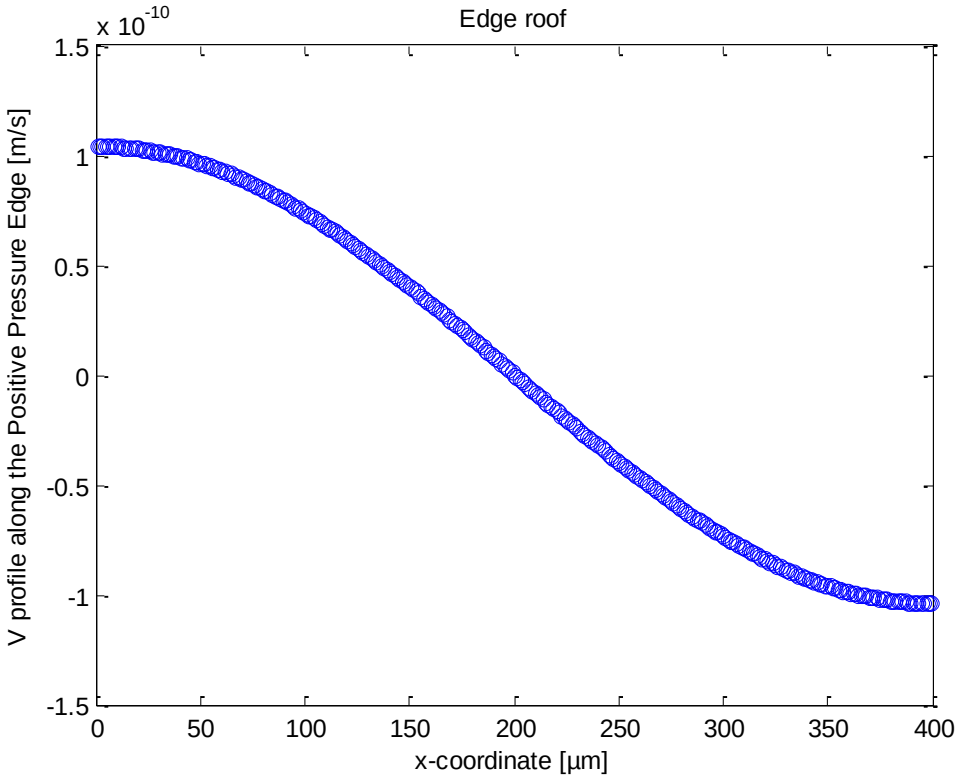

Figure 30. Velocity profile (integrand of the flow rate) at the upper boundary. It represents the velocities at which the fluid is escaping /entering the gel.

The error arises from differences in the integration points of the symmetrical solution. Therefore, we expect this error to be directly related to the number of mesh-refinements' performed. These errors were calculated with the standard number of refinements (NM) number of 5. However, we can test this relationship comparing the evolution of the error with NR. A number of refinements higher than 7 results in an inadequately long computational time.

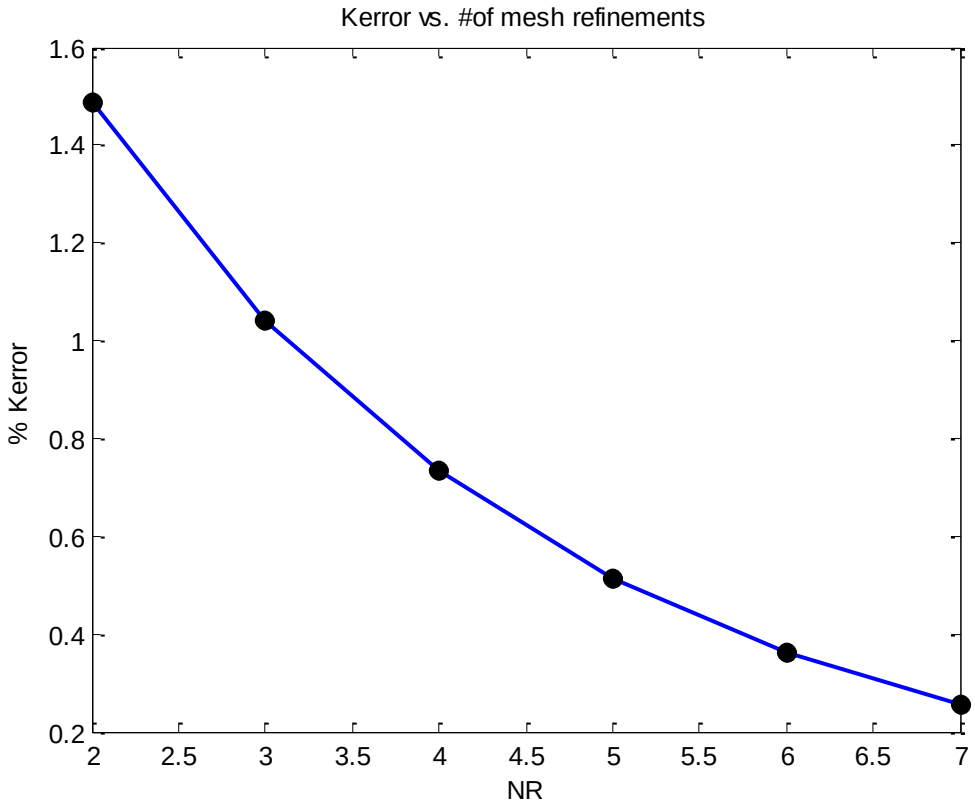

Figure 31. Correlation between the Kerror and the number of mesh refinements.

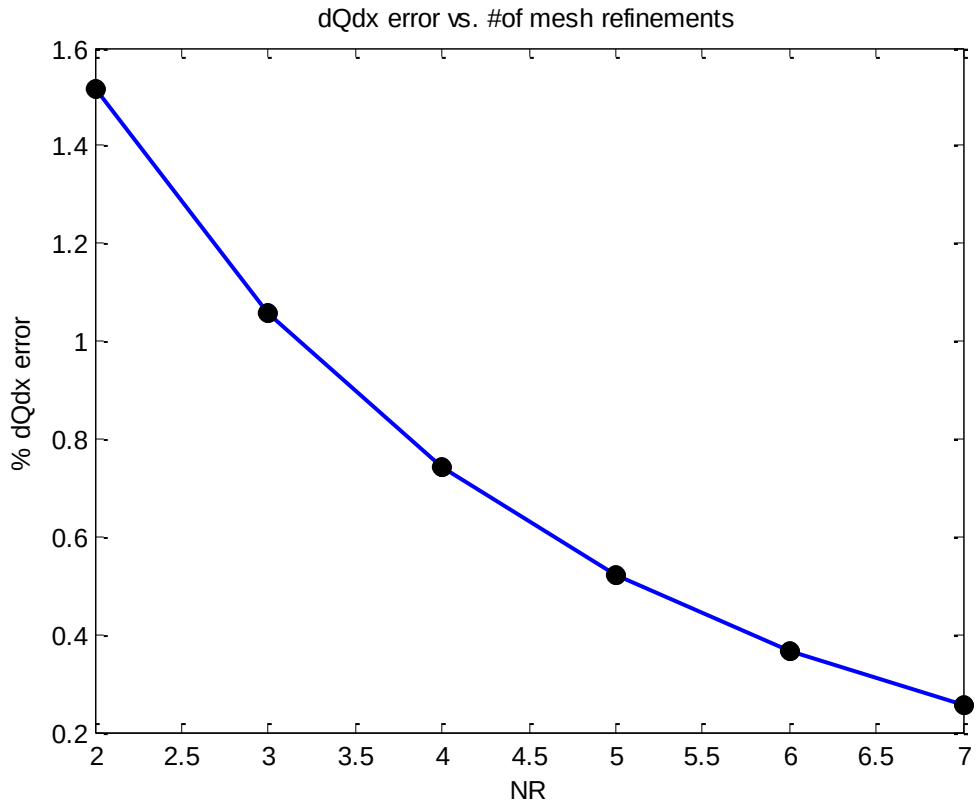

Figure 32. Correlation between the dQdx error and the number of mesh refinements.

We observe a substantial reduction of the error percentage as we increase the number of refinements. In fact, above four refinements the error is below 1%, which proves the high accuracy of the method employed.

Now that we have studied the proper operability of the tool, we proceed to investigate the best combination of parameters. In order to evaluate the dependency on each parameter, we will perform different simulations varying the magnitude of one of them while keeping the rest of them constant. The simulations are always done in the '*first stage'* of the model, which refers to the entry point of the flow to the device. Concerning the structural parameters, the following relationships were tested:

- **Flow rate loss ($dQpdx$) vs. Permeability of the fibrin gel (kg)**

Figure 33 illustrates the dependency of the amount of fluid exchanged between the channels and the diffusion coefficient of the gel. The results show the logarithmic plot of both factors, for the sake of clarity. As expected, a one-order-of-magnitude variation in the permeability factor results greatly influences the flow rate loss. The value of this parameter depends mainly on the composition of the gel. However, a mean permeability factor could be calculated for the gel and endothelial wall of the channels if it was finally added.

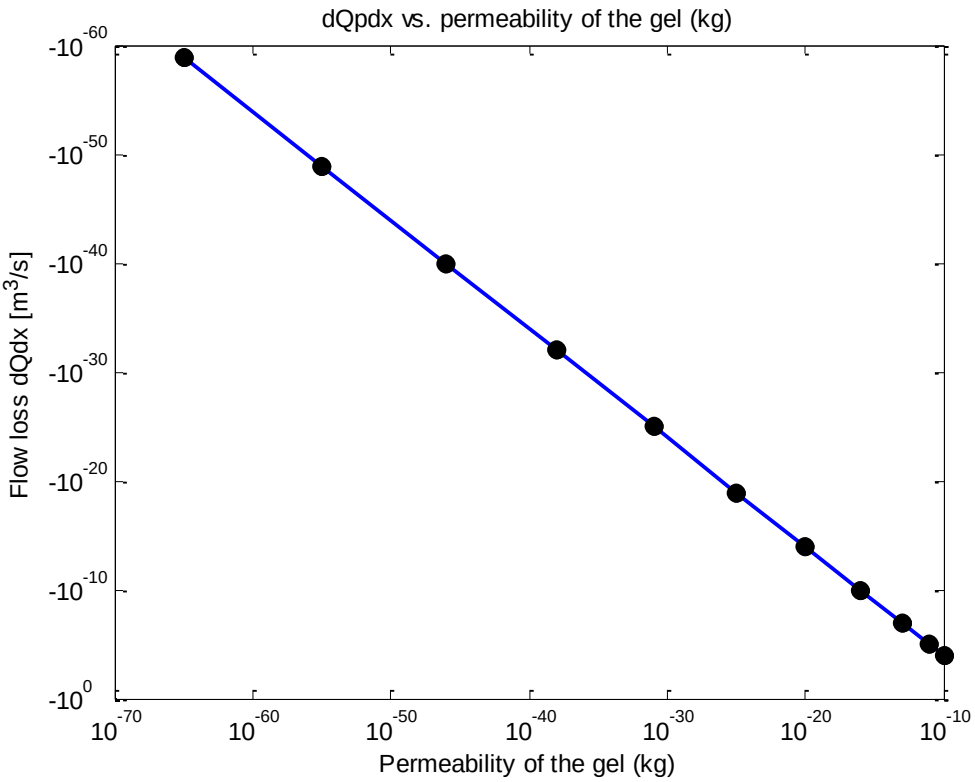

Figure 33. Fluid exchange (dQdx) vs permeability of the gel (kg).

- **Flow rate loss ($dQpdx$) vs. Separation between channel (W)**

The next correlation we may examine is the relationship between the amount of fluid that traverses the channels and the distance between them. The dependence between these two parameters is shown below (*Figure 34).*

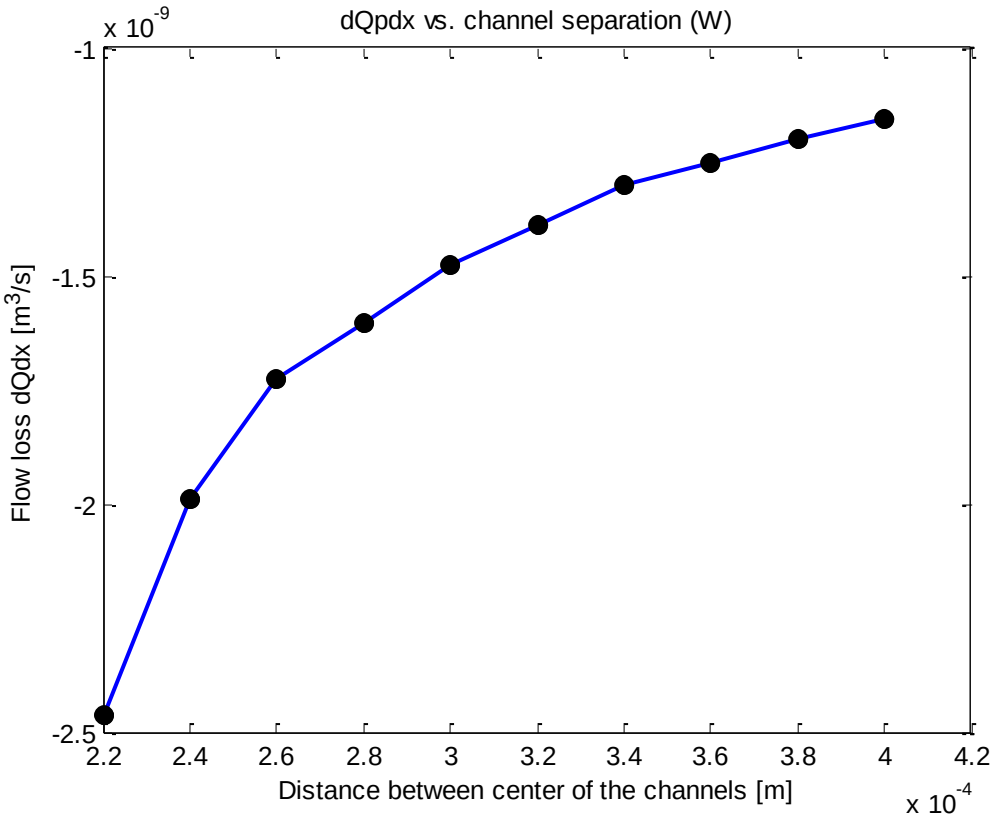

Figure 34. Fluid exchange (dQdx) vs distance between channels (W).

As we could expect, the results show a decrease in the fluid exchange as we increment the distance between the channels. This is due to the forces experienced by the fluid, which increase with the proximity of the source to the sink.

- **Velocity profile at the upper boundary vs. Thickness of the gel (H)**

The next important correlation could be the dependence of the flux across the upper boundary in relation to the increase in the gel's thickness. As we have repeatedly stated in the project, one of the main limitations of the first model is the impossibility to extend its height as much as wanted due to the decrease in flow rate at the top of the device. However, we need to analyze the extent of this limitation.

The following figure shows the velocity profile of the flux across the upper boundary as we increase the thickness of the gel. As we can see, there is a decrease of at least one order of magnitude in the velocity profile with each increment of the height from 100 µm to 600 µm.

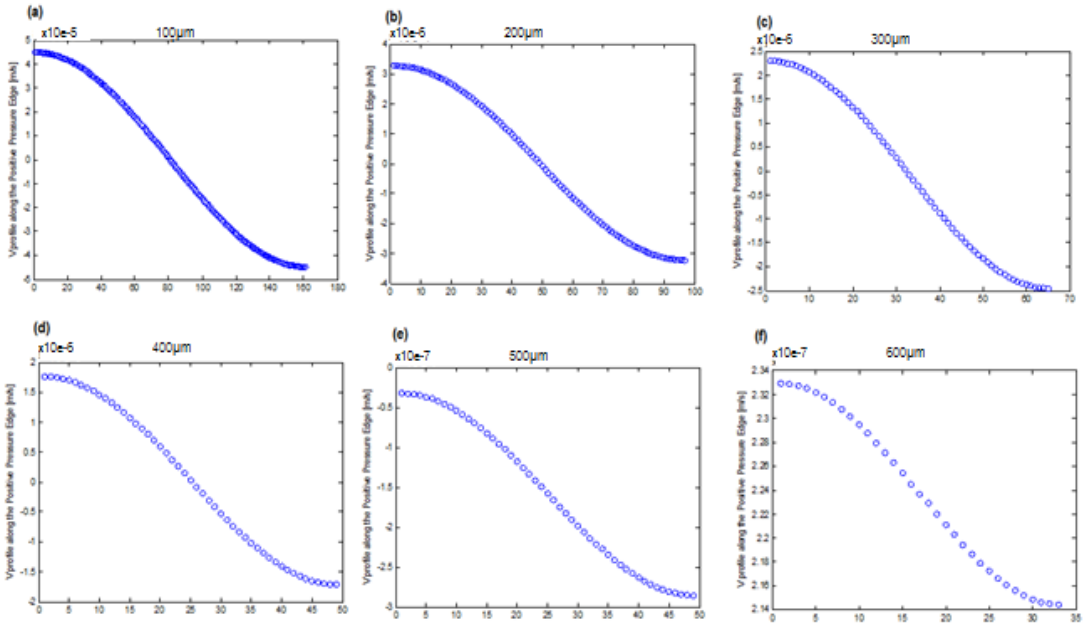

Figure 35. Velocity profile of the flux at the upper boundary for different thicknesses of the permeable gel ranging from 100 µm (a) to 600 µm (f) in increments of 100 µm.

- **Flow rate loss ($dQpdx$) vs. Side of the channel (D)**

The last parameter intrinsic to the geometry of the device is the hydrodynamic diameter of the channels. In the case of squared cross-sectional channels it refers to the side (D). Here, we show the relation between the lengthening of the side and the amount of fluid that escapes the positive conduct.

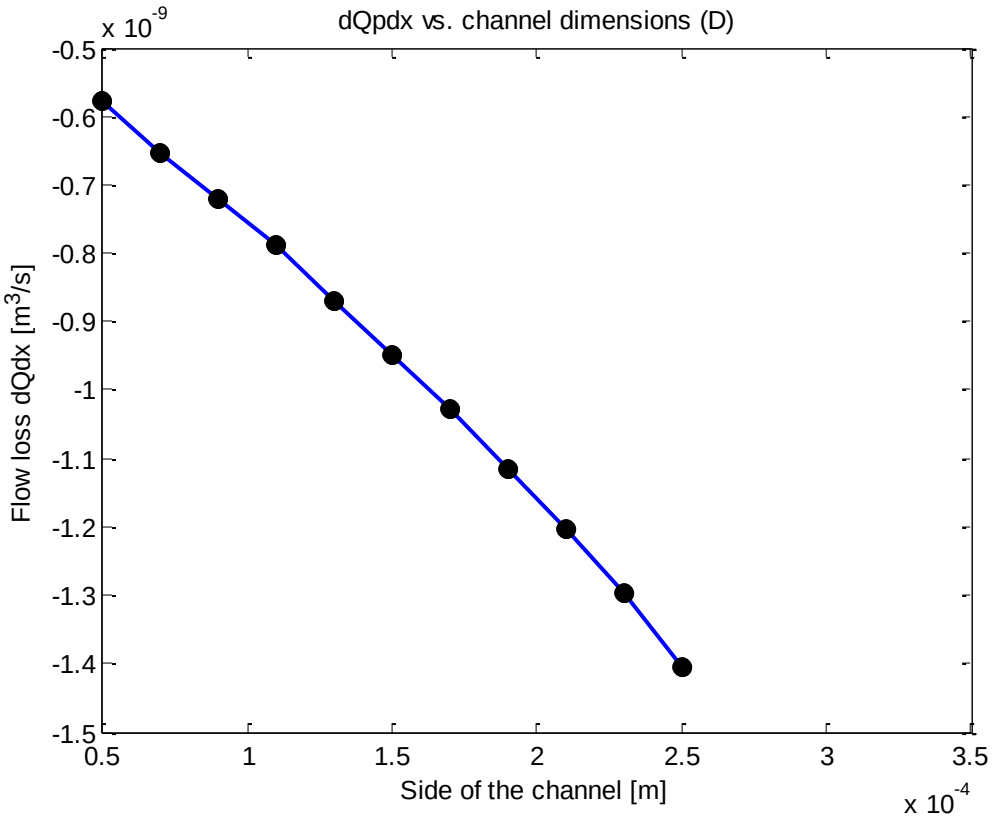

Figure 36. Plot of the flow loss versus the width of the channels. The distance between channels is kept constant, W = 80e-6 m.

The results show how the amount fluid that traverses the channels increases in magnitude as their cross-sectional area is increased. The negative sign of $dQpdx$ originates from the fact that the flow rate loss calculated refers to the positive channel (escaping fluid). As predictable from the analytical equations governing the flow, a larger cross-section of the channel leads to a greater flow loss.

- **Flow rate loss ($dQpdx$) vs. Pressure difference (ΔP)**

After reading through the model, one could think that one of the main parameters in the design of the device is the pressure difference between the channels. This pressure difference is responsible of the flux originated within the gel. It is reasonable to expect that it will have a significant influence in the amount of flow that traverses the channels. The relationship between both was carefully analyzed.

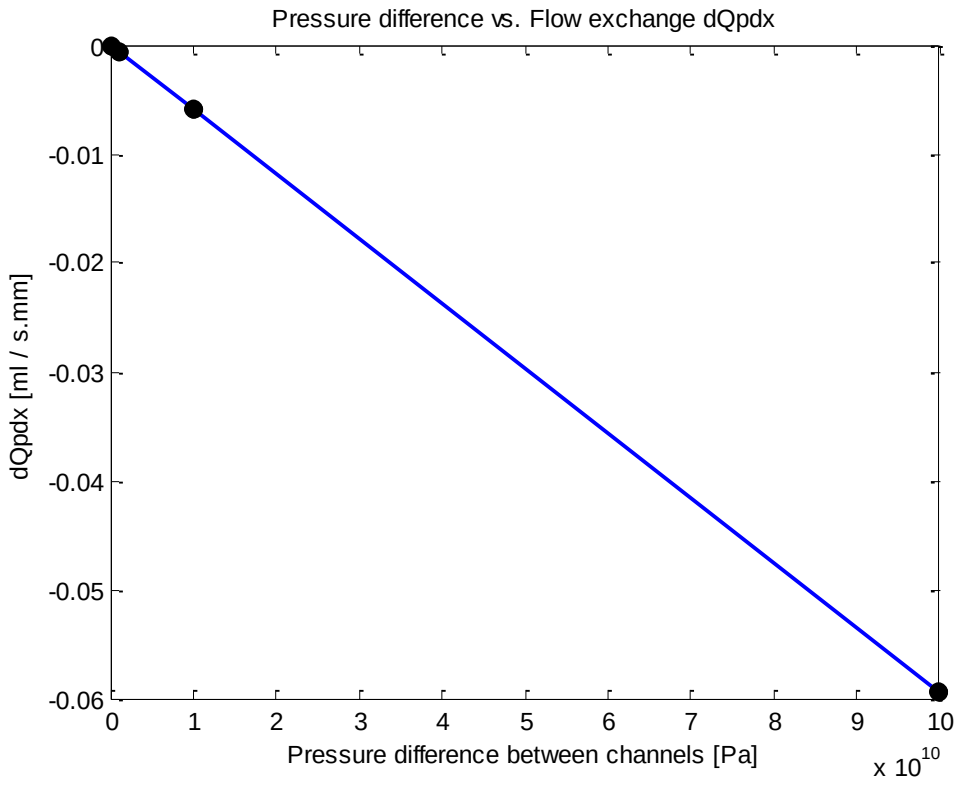

Figure 37. Linear dependence between the pressure difference and the flow loss.

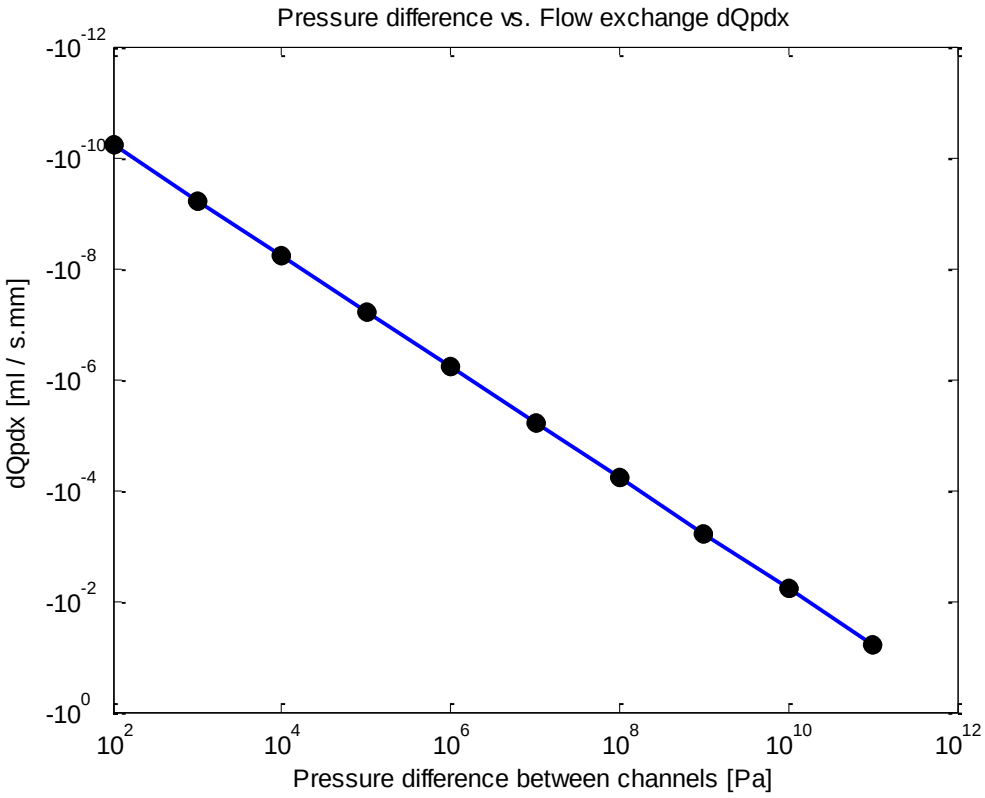

Figure 38. Logarithmic dependence between the pressure difference and the flow loss.

The graphs show a linear relationship between the difference in pressures and the amount of fluid that exits the positive channel. At this point, we could choose an appropriate pressure difference that originates the desired flux while conserving the integrity of the device. However, no evidence was found in literature about the necessary quantity of blood flow through the tissue. For the sake of simplicity, a pressure difference of 2000 Pa during the following simulations, which is close to the physiological value.

* It is important to mention that all the calculations were performed by assigning a pressure P = 0 to the top boundary of the gel. Besides, the positive channel was assigned a positive pressure value, whereas the negative one was given a symmetrical value with a negative sign. In a real design, the pressure at the top boundary would be expected to be the atmospheric pressure, (Pa). However, the model is designed to work in relation to this atmospheric pressure. That means, that whatever the pressure at the top is, that would set the zero in our model, and the pressures in the channels would be just relative pressures to this one. The value of the pressures in the channels do not need to have opposite signs (which is physically impossible), they just need to differ the same quantity above and below the top pressure. That way we would obtain a symmetrical flow going from the positive to the negative channel.

If the pressures in the channels were not symmetrical with respect to the pressure at the top, we would obtain non symmetrical flux profiles in which the source would be more powerful that the sink, or vice versa, and the fluid could go out or be sucked in from the upper layer, (air). Furthermore, if the pressure difference between the channels is not favorable compared to the pressure difference between any of the channels and the roof for the flow to be interchanged in that direction, we would have built a model with an undesired flow behavior, as it is illustrated in *Figure 39, 40, 41.*

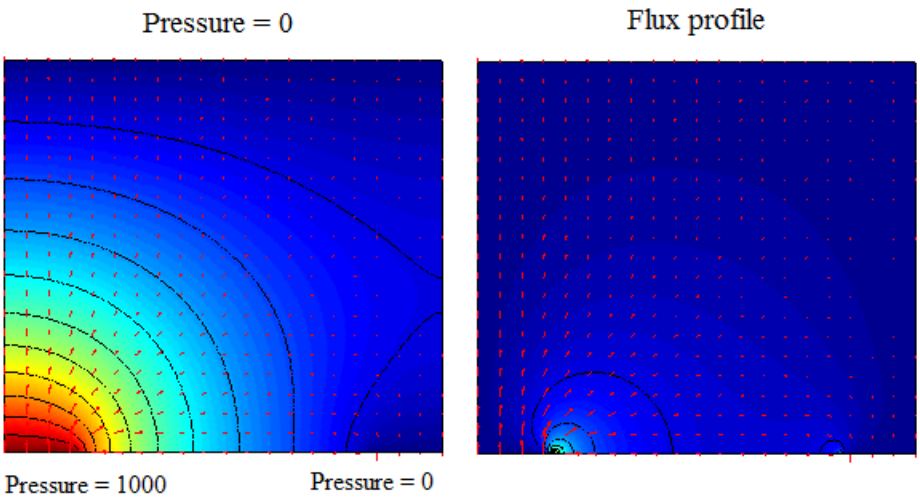

Figure 39. Pressure and velocity profiles when the negative and the top boundary are given the same pressure value.

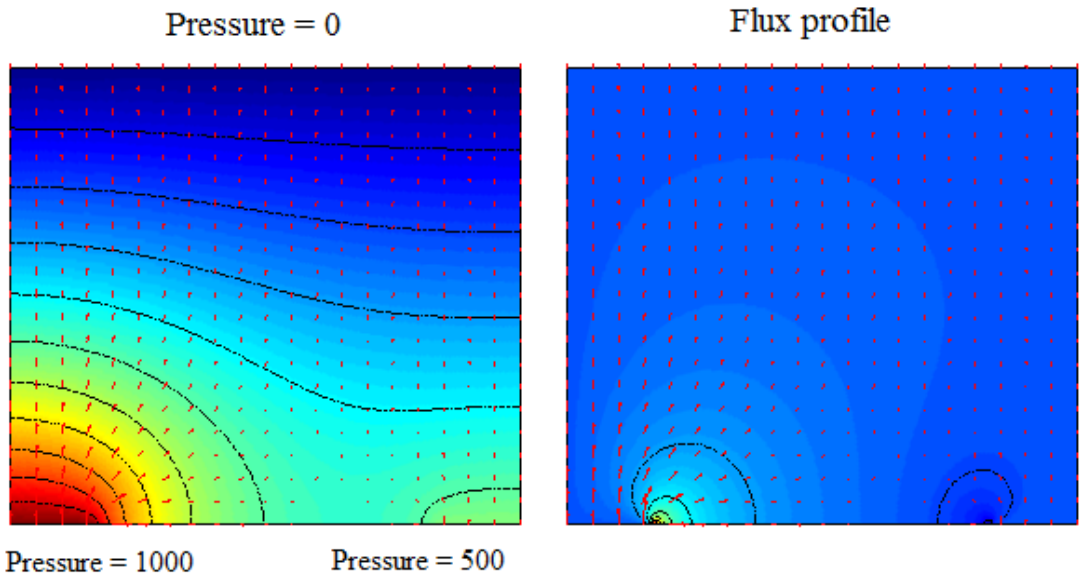

Figure 40. Pressure and velocity profiles when the channels do not carry symmetric pressures with respect to the top boundary.

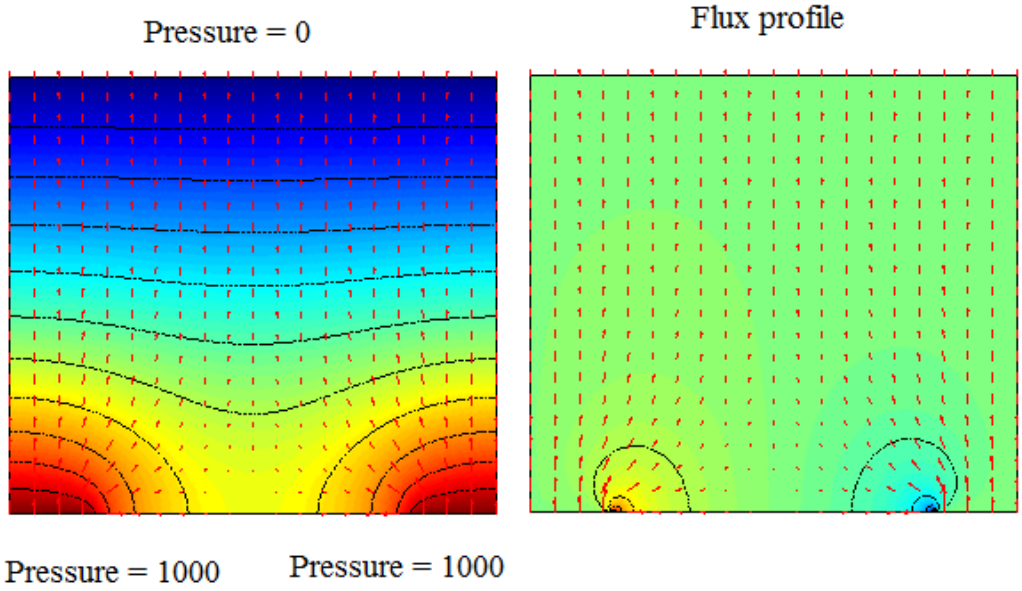

Figure 41. Pressure and velocity profiles when both channels' pressures are above the pressure at the upper boundary.

* Another important aspect to be taken into account is the maximum pressure that a microfluidic device can withstand before fluid loss or break out occurs. Literature shows studies about pressure-driven microdevices in which a maximum pressure of 2-4 Bars can be applied, which equals 100.000 - 200.000 Pa. (24)

Once the static behavior of the flow and the correlation among the defining parameters has been analyzed, the evolution of the flow along the longitudinal direction must be evaluated. As it has been explained, numerical methods to calculate the flow and pressure variations along the channels where applied implementing an ordinary differential equation's solving tool.

Figure 42, 43 show the evolution of the pressures along the channels in 1cm length.

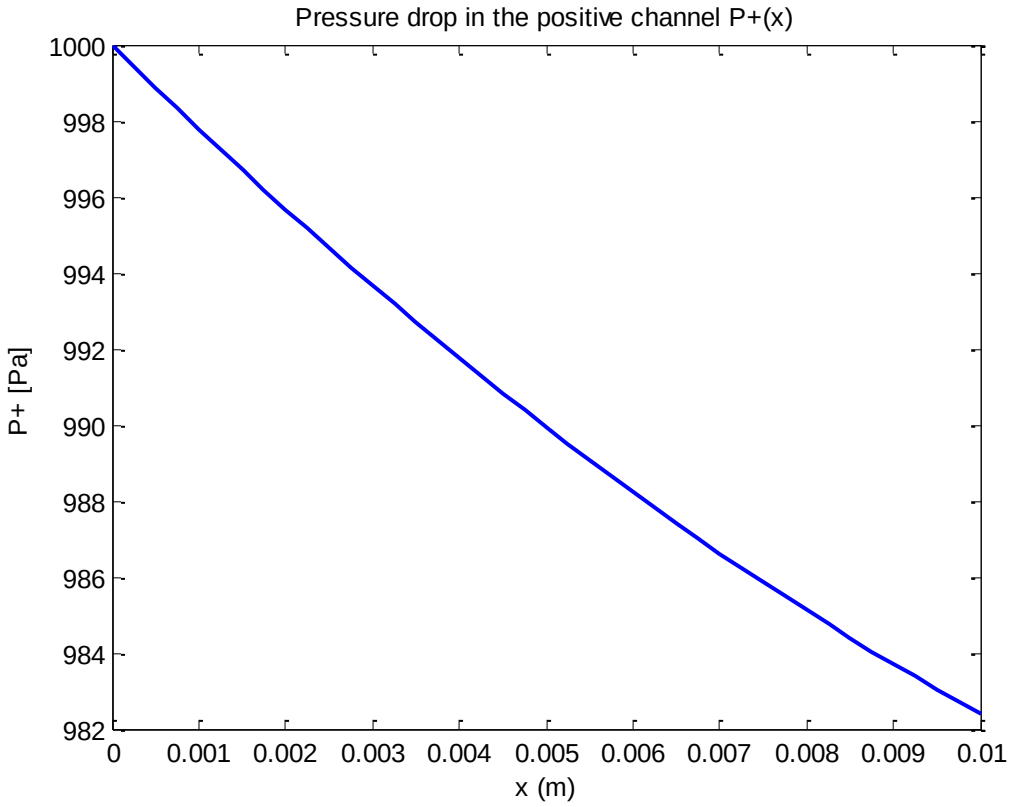

Figure 42. Illustration of the positive pressure drop along a 1 cm-long channel.

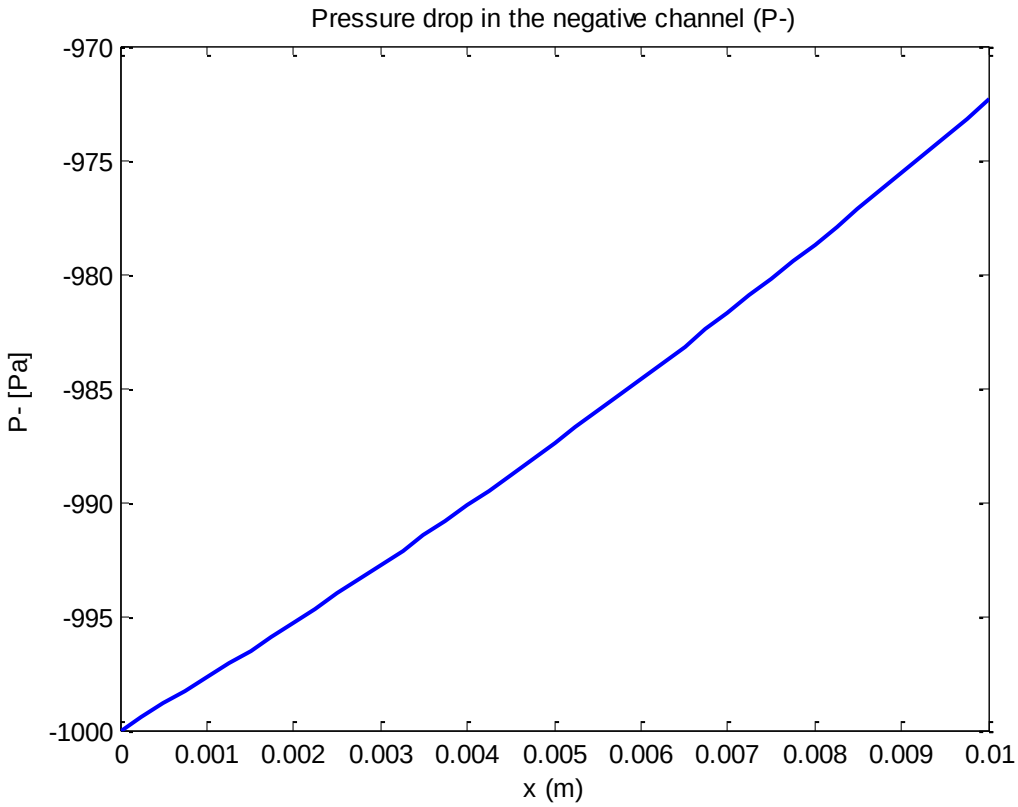

Figure 43. Illustration of the negative pressure variation along a 1 cm-long channel.

As we can see in the results, the positive pressure decays at a rate of 1800 Pa/m, which is 18 Pa/cm, due to the continues fluid loss experienced along the canals. In contrast, the negative pressure increases from -1000Pa to -977 Pa, almost at the opposite rate. As the model was designed to cover a total length of 1 cm, this drop in the pressure difference would probably not be significant to the exchange of fluid along the device. The pressure difference, which is responsible of the traverse of fluid between channels, drops 50 Pa in the control length.

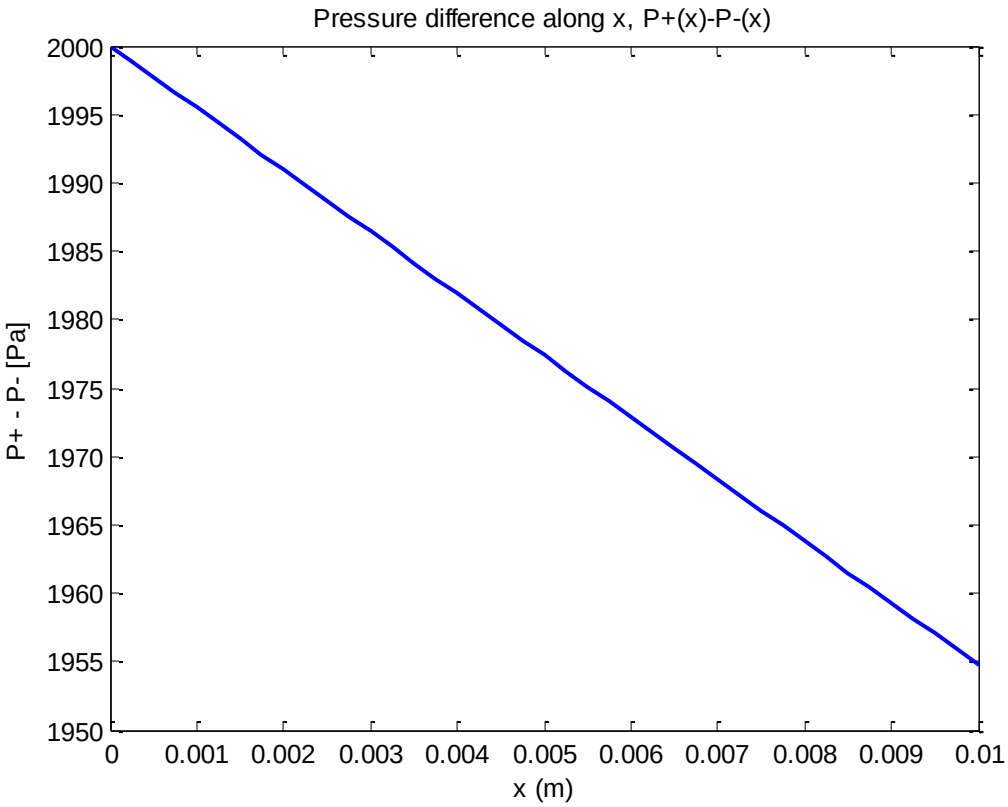

Figure 44. Pressure difference variation along the channels.

In order to gain visual information about the flow rate change in both pipes, the graphs of the changes experienced by the flow rates in the channels were plotted *(Figure 45, 46)*

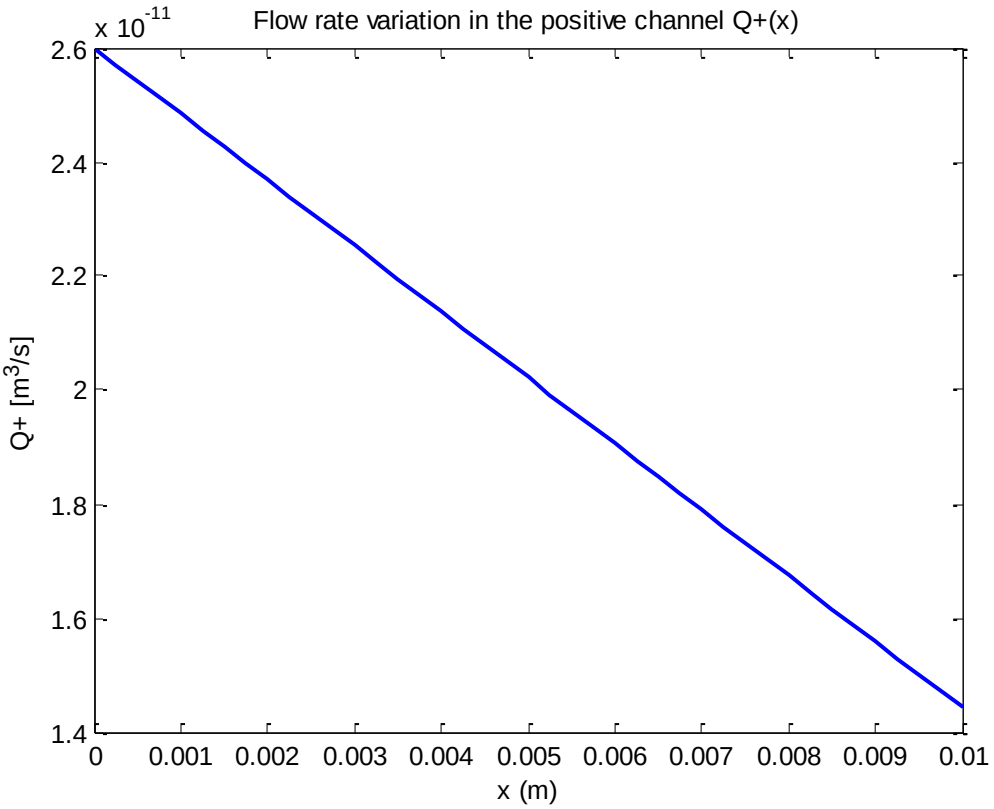

Figure 45.. Flow rate evolution along the 1cm-long positive channel.

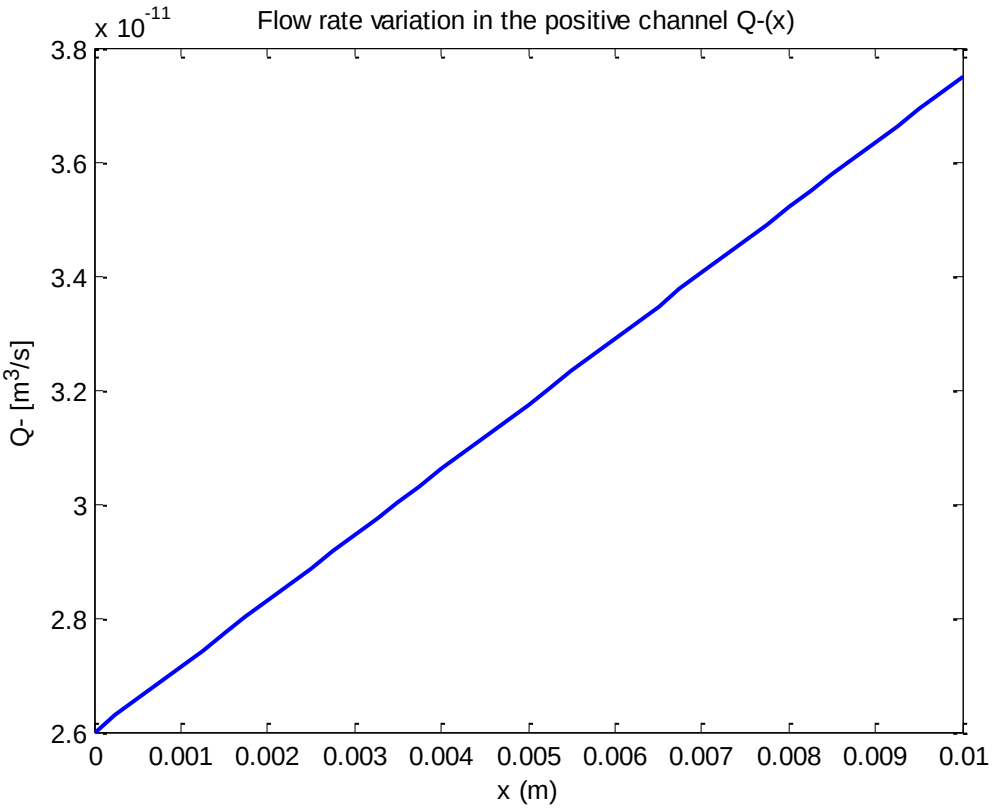

Figure 46. Flow rate evolution along the 1cm-long negative channel.

As we can infer from the graphs, a loss of fluid in the positive channel from the initial flow rate (Q_o = 2.6e-11 m^3/s) to a final flow rate (Q_f = 1.4e-11 m^3/s) along the positive pipe can be appreciated, which corresponds to the increment in fluid rate in the parallel one. However, we are heavily interested in the variation of the flow rate loss trough the permeable gel, which is the nourishment source for the cultured cells. The variation of this factor along the longitudinal direction is crucial to ensure a proper and sufficient nutrient supply to the cells. The decay in the pressure difference between the channels might meaningfully affect this flow, and it could limit the culture surface available for our experiment. *Figure 47* shows this variation along the gel.

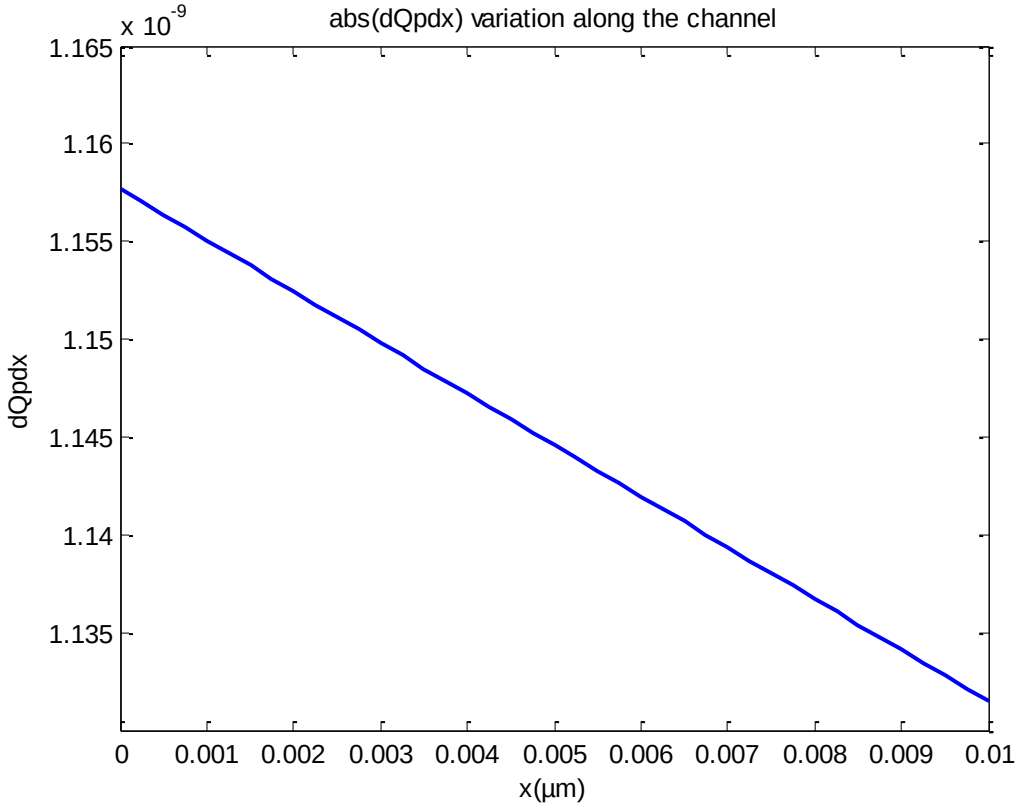

Figure 47. Variation of the flow rate loss at the 1cm-long positive channel.

The results show a decrease of 0.03 µl/m, which might be crucial for the integrity of the culture under homogeneous conditions.

4.2. Improved model

The workability of the improved model was tested for the same configuration of parameters described before, with the intention to be able to compare both approaches.

First, the variation of the pressures along the channels was plotted for the same length extension (*Figure 48, 49).*

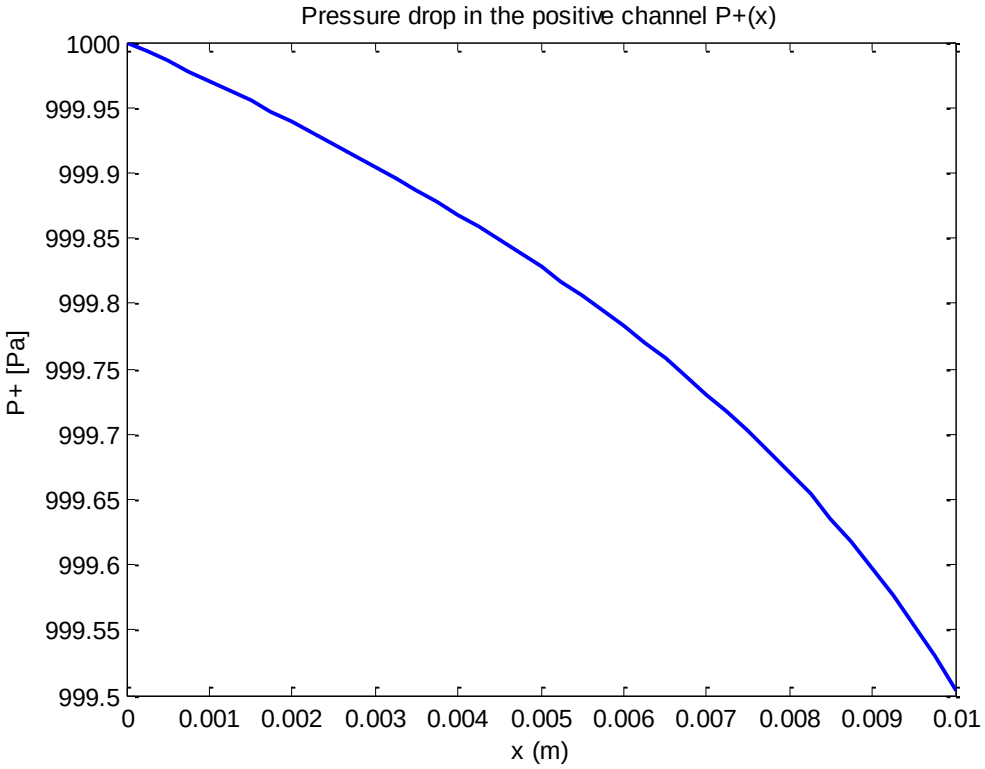

Figure 48. Illustration of the negative positive drop along a 1 cm-long channel.

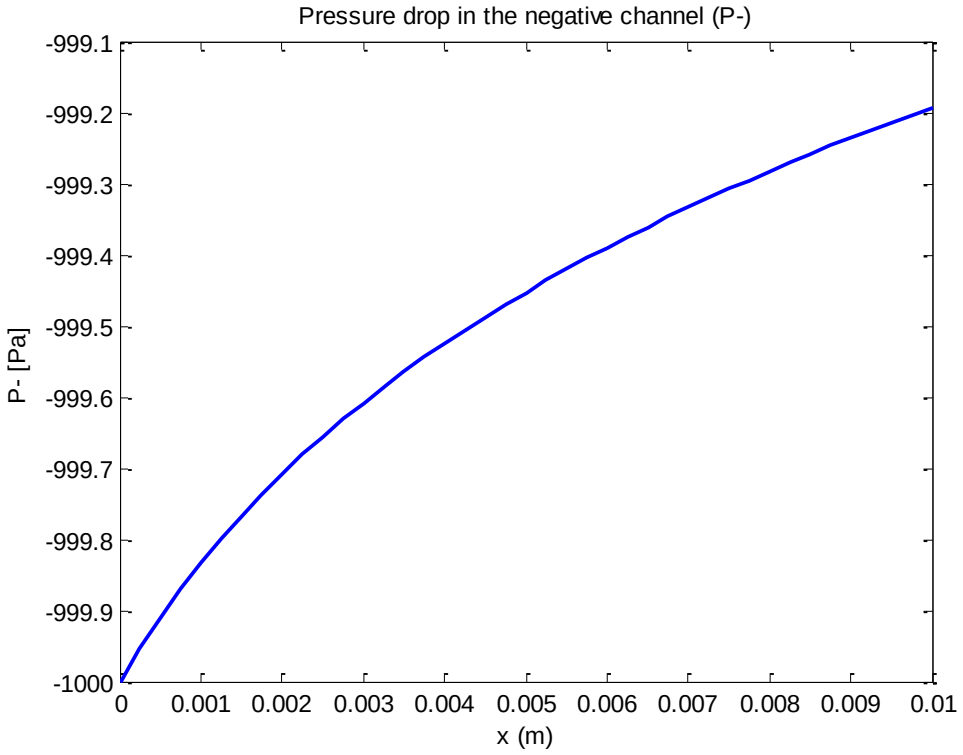

Figure 49. Illustration of the negative pressure variation along a 1 cm-long channel.

The results show a much smaller pressure variation along the channels. In 1 cm, the positive channel experiences a pressure drop of just 0.5 Pa in favor of the negative one. As expected, the variation in the cross-sectional area of the channels as the fluid is gained / lost has a crucial influence, reducing the pressure drop. This leads to a more important result, which is the stable pressure difference between the canals, *(Figure 50)*

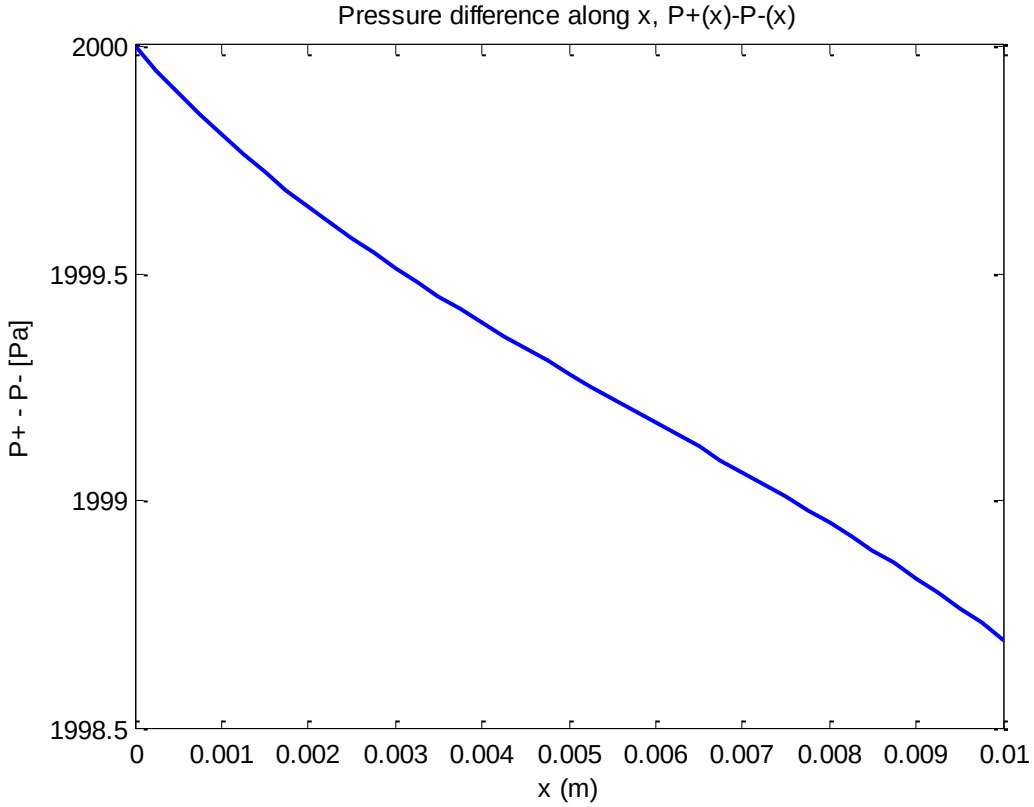

Figure 50. Pressure difference variation along the channels.

As we can check, the pressure difference between both channels varies 1.5 Pa along the whole device, in contrast to the 50 Pa drop in the previous model. This is a promising result regarding the objective of the improved model. The area of the positive channel was reduced by a factor of three according to the flow rate loss, whereas the cross-section of the negative channel was increased by the same factor to counteract the effect of the incoming external fluid. The results show a stabilized pressure difference variation. Next, the flow rates along the channels was calculated and plotted for the sake of comparison. *Figure 51* illustrates the outcome of the simulation.

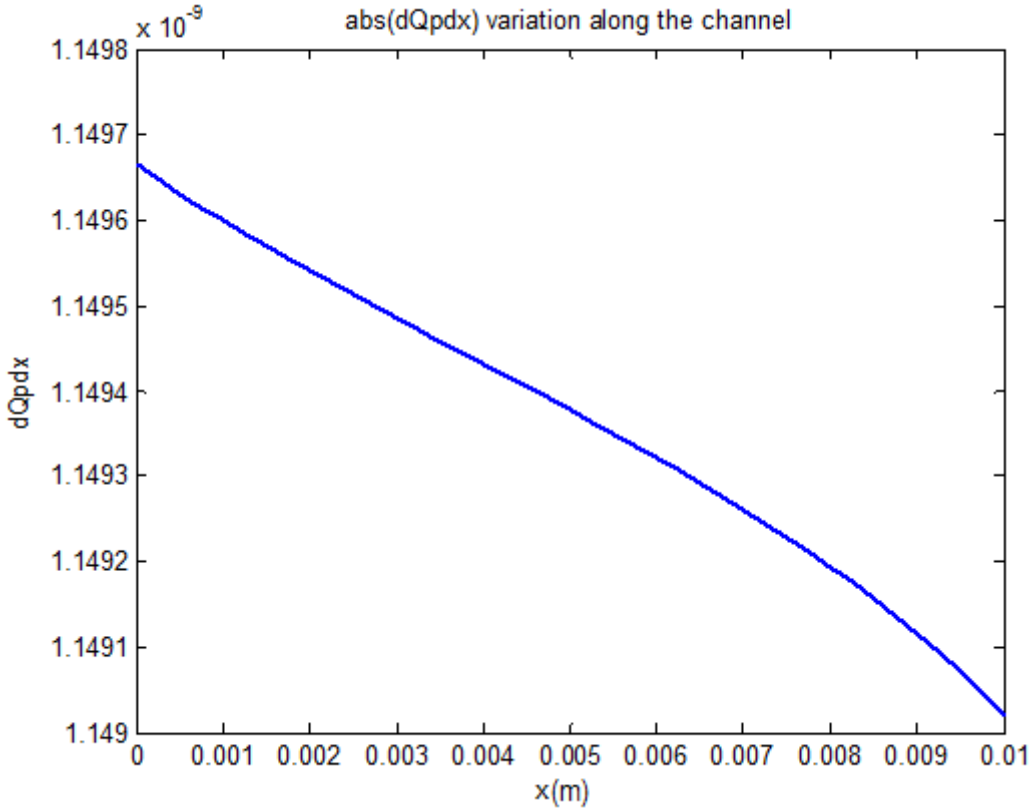

Figure 51. Variation of the flow rate loss at the 1cm-long positive channel.

The above figure reaffirms the successful results originated from the pressure-difference variation calculation. The stabilization of the pressure-difference between channels leads to a nearly homogeneous flow rate loss along the pipes, decreasing by 0.009 μl/m, in contrast with the value of 0.03 μl/m calculated for the first model. This achievement enormously expands the possibilities of the microchip, enabling a model of extended culturing area that maintains homogeneous conditions for the cultured cells. A further simulation was performed in a 10cm long device. Results are illustrated in *Figure 52.*

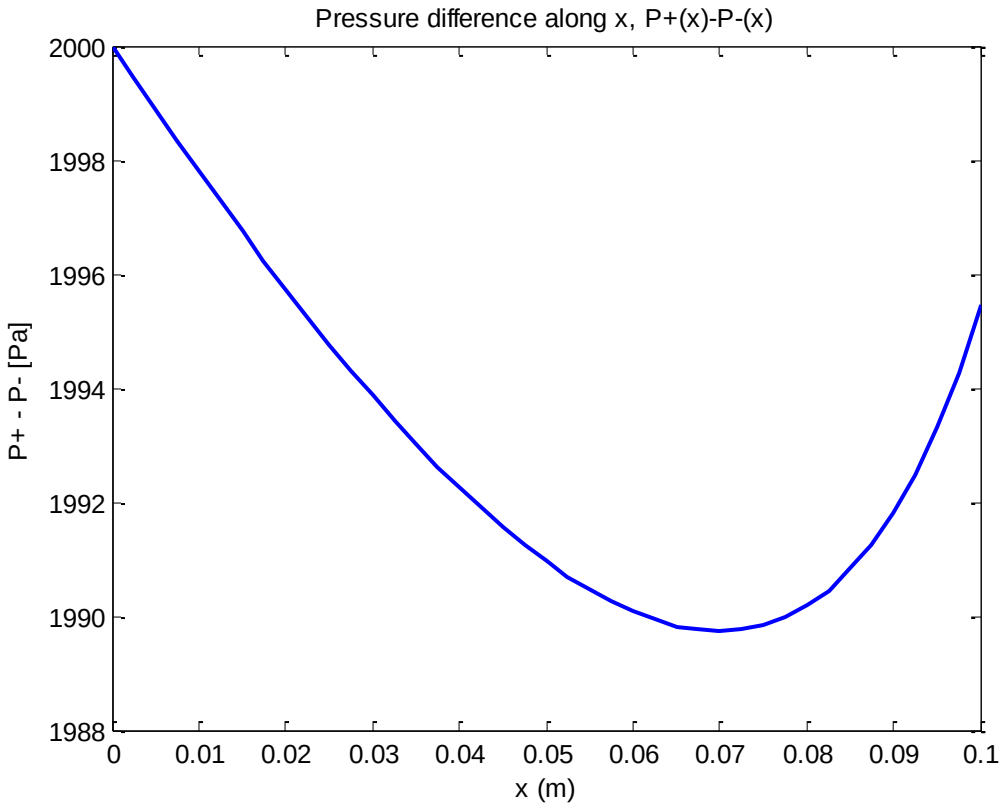

Figure 52. Pressure difference variation along 10cm-long channels.

As it may be observed, the pressure difference between the channels suffers an unpredictable turn over at the 7cm mark. This is originated at the moment when the flow rate in the positive channel reaches a zero value, which means that the fluid travelling along this pipe has utterly been traversed to the parallel one. However, this is just a matter of the initial conditions of the simulation. The delightful result from the previous recreation relies on the pressure difference evolution, which once again is show to be fairly constant along the channels.

Finally, a code to plot the solution to the pressure field in the extended model were the channels are engraved into the gel was developed. Even though the pressure results correspond to the simplified model in which the channels are engraved below the permeable gel, a simulation of the picture that the control surface of the extended model would have is shown in *Figure 53.*

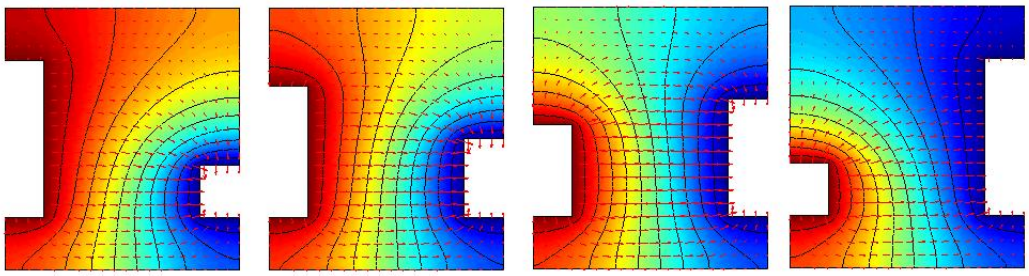

Figure 53. Simulation of the pressure field in the cross-sectional-varying channels along x.

5. CONCLUSION

5. Conclusion

In this project, a programming tool was developed to simulate the design of a microfluidic chamber to grow skin-on-a-chip. Making use of this tool, two approaches were modeled, discussed and compared in order to describe the best configuration of parameters for the design of the device.

1. The main goal of this work was to develop a flexible, programmable computational tool able to predict the workability of a modeled microfluidic chamber by numerical methods. To conceptualize a new model, it is necessary to describe its physical structure and the governing parameters of the flow. The program was shown to own a versatile and adaptable interface that treats carefully the statement of the problem and responds adequately to the input arguments.

2. The tool developed is able to solve the problem for any imaginable geometry providing accurate, errorless numerical results. It also makes available a wide range of graphical representations of the solutions that ease the understanding of the results to the user, as well as the possibility to test each parameter in the design independently.

Two different models were developed for the design of a microfluidic chamber with proper fluid behavior to grow skin-on-a-chip. Several computational approaches were used in order to predict the behavior of the pressure gradients, flow rates and diffusion profile in the devices.

A basic prototypical structure composed of a set of microchannels to nourish a permeable fibrin gel through which fluid can diffuse was defined. The workability of the model was tested.

An improved model attempting to overcome the limitations posed by the first approach was developed and analyzed.

3. A primitive model of the skin-on-a-chip was engineered. The design included a single set of microfluidic channels aiming for nutrient supply to the populating cells of a permeable fibrin gel on top of it. The approach includes several advantages over more complex designs, including a simplified structure to be microfabricated and cheaper cost of manufacturing due to the reduced amount of materials and microfabrication procedures needed. On the contrary, it would pose limitations regarding the maximum possible thickness of the culture, or the available culturing area in the longitudinal direction.

4. An improved model was described and tested, composed by a set of alternating parallel microfluidic channels for nourishment and trash removal respectively whose cross-sectional area varies along the longitudinal direction to compensate the fluid loss and maintain the pressure drop minimum. The design showed positive results fulfilling this objective, and providing an extended available culturing area in comparison with the first model.

Note: The codes developed in this project are meant to be open-source.
Anybody interested, may contact this email: *pablo.tostado@yahoo.es*

References

1. Palaniyappan V, Jagannadham P, Anusuri HSP, Paturi UM, Kunkala S, Kothandam HP. ORGAN-ON-A-CHIP TECHNOLOGY—A SUBSTITUTE TO ANIMAL TESTING.
2. Science FoEaa. Losses in Pipes.
3. Wikswo J. The Homunculi and I- Lessons from Building Organs on Chips 2013. Available from: https://www.youtube.com/watch?v=4ht3m6p8iZ0.
4. Herper M. The Decline Of Pharmaceutical Research, Measured In New Drugs And Dollars. 2011.
5. Hamilton G. Your body in a microchip 2013. Available from: https://www.youtube.com/watch?v=cn9Q4c3dXGU.
6. Chmielowiec J, Borowiak M. In vitro differentiation and expansion of human pluripotent stem cell-derived pancreatic progenitors. The review of diabetic studies: RDS. 2013;11(1):19-34.
7. Matther JP. Introduction to Cell Tissue Engineering2000.
8. Genovese J, Cortes-Morichetti M, Chachques E, Frati G, Patel A, Chachques JC. Cell based approaches for myocardial regeneration and artificial myocardium. Current stem cell research & therapy. 2007;2(2):121-7.
9. Chin CD, Khanna K, Sia SK. A microfabricated porous collagen-based scaffold as prototype for skin substitutes. Biomedical microdevices. 2008;10(3):459-67.
10. Huh D, Hamilton GA, Ingber DE. From 3D cell culture to organs-on-chips. Trends in cell biology. 2011;21(12):745-54.
11. Cheng S-Y, Heilman S, Wasserman M, Archer S, Shuler ML, Wu M. A hydrogel-based microfluidic device for the studies of directed cell migration. Lab on a Chip. 2007;7(6):763-9.
12. Huh D, Matthews BD, Mammoto A, Montoya-Zavala M, Hsin HY, Ingber DE. Reconstituting organ-level lung functions on a chip. Science (New York, NY). 2010;328(5986):1662-8.
13. Alcendor DJ, Block III FE, Cliffel DE, Daniels JS, Ellacott KL, Goodwin CR, et al. Neurovascular unit on a chip: implications for translational applications. Stem cell research & therapy. 2013;4(Suppl 1):S18.
14. Kim HJ, Huh D, Hamilton G, Ingber DE. Human gut-on-a-chip inhabited by microbial flora that experiences intestinal peristalsis-like motions and flow. Lab on a Chip. 2012;12(12):2165-74.
15. Panoskaltsis-Mortari A, Weiss DJ. Breathing new life into lung transplantation therapy. Molecular Therapy. 2010;18(9):1581.
16. Weis JM, Staicu SA, Chase KS. Lung-on-a-Chip Microdevice, Right Ventricular Dysfunction as a Predictor of Survival, and Lung Ultrasound in Community-acquired Pneumonia. American journal of respiratory and critical care medicine. 2013;188(8).
17. Canton I, Cole DM, Kemp EH, Watson PF, Chunthapong J, Ryan AJ, et al. Development of a 3D human in vitro skin co-culture model for detecting irritants in real-time. Biotechnology and bioengineering. 2010;106(5):794-803.
18. Ucko DA. Living Chemistry.
19. Chiu CL, Hecht V, Duong H, Wu B, Tawil B. Permeability of three-dimensional fibrin constructs corresponds to fibrinogen and thrombin concentrations. BioResearch open access. 2012;1(1):34-40.
20. G. B. Introduction to Fluid Mechanics2000.

21. Batchelor G. Slender-body theory for particles of arbitrary cross-section in Stokes flow. Journal of Fluid Mechanics. 1970;44(03):419-40.
22. Williams S, Fatah K, Hjemdahl P, Blombäck M. Better increase in fibrin gel porosity by low dose than intermediate dose acetylsalicylic acid. European heart journal. 1998;19(11):1666-72.
23. Meana A, Iglesias J, Del Rio M, Larcher F, Madrigal B, Fresno M, et al. Large surface of cultured human epithelium obtained on a dermal matrix based on live fibroblast-containing fibrin gels. Burns. 1998;24(7):621-30.
24. Kohl M. Fluidic actuation by electrorheological microdevices. Mechatronics. 2000;10(4–5):583-94.